RUTHENIUM-TRIS(PYRAZOLYL)METHANE COMPLEXES AS POTENTIAL CANDIDATES FOR CANCER CHEMOTHERAPY AGENTS

By

Jesse M. Walker

Submitted to

The Department of Chemistry, Lakehead University,

in Partial Fulfillment of the Requirements for the Degree of

Master of Science

Supervisors: Dr. G. J. Spivak and Dr. C. Gottardo

Department of Chemistry, Lakehead University

Thunder Bay, Ontario, Canada, P7B 5E1

August 2009

To my family Karen, Bob, Casey and Laura whose continuous love and support has been the instrument of my success. Thank you, I love you all!

I would also like to dedicate this work to Kol McKay, Sybil Lindeboom, Wilma Marriott and Rose Walker who have all faced this horrible disease. Your courage and bravery has been a tremendous inspiration for this project!

Abstract

A convenient and versatile route to the synthesis of $[(tpm)RuCl(LL)]PF_6$ (where: tpm= tris(pyrazolyl)methane; LL= 2(MeCN) (**1**), 2(DMSO) (**2**), 2(P(OMe)$_3$) (**3**), 2(MePPh$_2$) (**4**), Ph$_2$P(CH$_2$)$_n$PPh$_2$ (n= 1 (**5**), 2 (**6**), 3 (**7**), 4 (**8**)) was developed. In contrast, attempts to synthesize $[(tpm)RuCl(en)]PF_6$ and $[(tpm)RuCl(dab)]PF_6$ (where en= ethylenediamine and dab= 1,2-diaminobenzene) by various methods were unsuccessful under the conditions explored. The MeCN ligands of complex **1** were substitutionally inert, however, under forcing conditions the DMSO ligands of complex **2** were displaced by chelating 1,2-bis(diphenylphosphino)ethane to produce complex **6**. Structural characterization of compounds **1-8** was performed by NMR spectroscopy, and an X-ray diffraction analysis of complex **7** provided additional evidence for the proposed structures.

Compounds **1-8** were compared against established anticancer agents cisplatin and doxorubicin for potential anticancer properties in the MCF-7 and HeLa cancer cell lines using the 3-(4,5-dimethylthiazol-2-yl)-2,5-diphenyltetrazolium bromide (MTT) cell viability assay. It was found that complexes **1** and **2** did not have effective inhibitory concentrations (IC$_{50}$) within the concentrations tested and complex **3** showed moderate antiproliferative activity. However, the phosphine complexes **4-8** exhibited remarkable antiproliferative effects in both cell lines with IC$_{50}$ values lower than that of cisplatin and close to the values for doxorubicin. Structure-activity relationships are discussed.

Acknowledgements

First and foremost, I would like to thank my primary supervisor and good friend, Dr. Greg Spivak, who introduced me to the fascinating world of coordination chemistry and bioinorganic chemistry. I consider myself very lucky to have had the chance to work in his laboratory, and truly believe that the completion of this degree is a result of Greg hiring me as a research assistant five years ago. Thanks for everything Greg!

I would also like to thank Dr. Christine Gottardo, Dr. John Th'ng and Dr. Mary-Lynn Tassotto. This project would not be possible without the help and guidance of these talented researchers. I wish you all the best in your future endeavors and would consider it a privilege to work with you in the future.

Acknowledgement must also be given to Dr. Brian R. James, who served as my external reviewer. His corrections and suggestions have contributed greatly to this manuscript.

Roxanne Pycko and Alexis McEwan performed all of the MTT assays (over 60 trials in total!!) for this project. Thank you both for all your hard work.

Next, I would like to thank Tim Larocque, Mike Beach, Justin Deagle and the other people with whom I have shared the lab. CB2031 has seen lots of fun over the past few years. I owe that to the friends that I have made there over the years along with the other students in the chemistry program. Good luck in the 'big smoke' Timbo!

All of the faculty and staff of the chemistry department deserve special mention, for they have provided me with an excellent undergraduate and graduate experience.

Last but not least, I would thank HSB and friends who have kept things interesting and creative outside of the lab. HSB alright!!

Contents

List of Figures

List of Tables

List of Schemes

Abbreviations

Ac = acetyl group

acac = acetylacetonate

ATP

bipy = 2,2'-bipyridine

br = broad

COD = 1,5-cyclooctadiene

D = deuterium, ^2H

dab =1,2-diaminobenzene

dach = 1,2-diaminocyclohexane

DMSO = dimethylsulfoxide, $SO(CH_3)_2$

DNA = deoxyribonucleic acid

dppb = 1,4-bis(diphenylphosphino)butane

dppe = 1,2-bis(diphenylphosphino)ethane

dppm = bis(diphenylphosphino)methane

dppp = 1,3-bis(diphenylphosphino)propane

en = ethylenediamine, $NH_2(CH_2)_2NH_2$

Et = ethyl group

HeLa = human cervical cancer cell line

HIV = human immunodeficiency virus

HMG = high mobility group (proteins)

hr = time in hours

Hz = Hertz, cycles per second

IC_{50} = inhibitory concentration (50%)

m = multiplet

MCF-7 = human breast cancer cell line

Me = methyl group

MTT = 3-(4,5-dimethylthiazol-2-yl)-2,5-diphenyltetrazolium bromide

NA = not available

NADH = nicotinamide adenine dinucleotide

NADPH = nicotinamide adenine dinucleotide phosphate

NMR = nuclear magnetic resonance

p-cymene = 1-methyl-4-isopropylbenzene

Ph = phenyl group, C_6H_5

ppm = parts per million

PTA = 1,3,5-triaza-7-phosphaadamantane

Pz = pyrazolyl

R(') = alkyl or aryl group

RAPTA = ruthenium-arene 1,3,5-triaza-7-phosphaadamantane compound

RNA = ribonucleic acid

s = singlet

tmeda = N,N,N',N'-tetramethylenediamine

tpm = tris(pyrazolyl)methane

Å = angstroms, 10^{-10} m

$\{^1H\}$ = proton decoupled

2D-NMR = two dimensional nuclear magnetic resonance

1. Introduction

1.1 General Introduction to Metals in Medicine

A common misconception that plagues the development of new innovative pharmaceuticals is that these compounds must be composed of an organic framework to be compatible with biological systems [1]. Additionally, metals and their complexes are often associated with severe toxicity despite the gram-scale utilization of iron, copper and zinc in many biological processes occurring in the human body [1]. Although the vast majority of compounds that are investigated for beneficial biological activity are in fact organic molecules, there is a rapidly growing number of metal-based compounds that display remarkable, and often times unprecedented, action against a wide variety of diseases [2].

The spectrum of biological disorders that are positively affected by coordination and organometallic compounds is rather impressive. Examples of metal compounds that possess novel biomedical applications include: various gold compounds used to treat arthritis, malaria and asthma; zinc, palladium and ruthenium compounds that display anti-HIV properties; and a plethora of metal-based complexes used as diagnostic imaging agents [3]. In fact, the notion of treating various ailments with metal-based compounds began in ancient times; however, these treatments were based on the superstitious philosophies that ancient cultures maintained regarding these extraordinary materials [3]. Indeed, modern medicinal bioinorganic chemistry has become a well-established

discipline. Much of the development and expansion of inorganic therapies has emanated from the astonishing clinical success of cisplatin, a platinum metallopharmaceutical, used in the treatment of cancer.

1.2 Cisplatin: From Serendipity to the Forefront of Cancer Chemotherapy

The discovery of the biological activity of cisplatin has had a profound impact on both the chemotherapeutic treatment of cancer and the development of innovative anticancer compounds. The molecular structure of cisplatin (Figure 1) is a simple square-planar coordination complex consisting of a platinum(II) centre with two chloride ligands in a *cis* relationship and two ammines completing the remaining coordination sites [4]. The introduction of cisplatin to clinical use, in 1978, armed clinicians with the means to treat malignancies that were previously untreatable [4]. The truly incredible chemotherapeutic importance of cisplatin is exemplified by the fact that this platinum coordination compound is used in the treatment of more than 70% of all cancer patients [3].

$$Cl\diagdown_{Pt}\diagup NH_3$$
$$Cl\diagup \diagdown NH_3$$
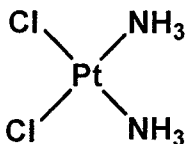
Figure 1. Molecular structure of cisplatin [4].

Although the mode of action of cisplatin has been debated in the literature for many years, it is now generally accepted that cellular responses to DNA-

cisplatin interaction that lead to apoptosis are responsible for the anticancer properties of this complex [5]. Cisplatin is administered intravenously, and is believed to remain predominantly unchanged outside the cell where the chloride concentration of about 100 mM is large enough to inhibit ligand substitution [4]. However, once the compound enters the cell, intracellular chloride concentrations, estimated to be less than 5 mM in some cells, are greatly reduced allowing for aquation (Scheme 1). It is in these cationic forms that the drug may form DNA adducts and can elicit an apoptotic response [4].
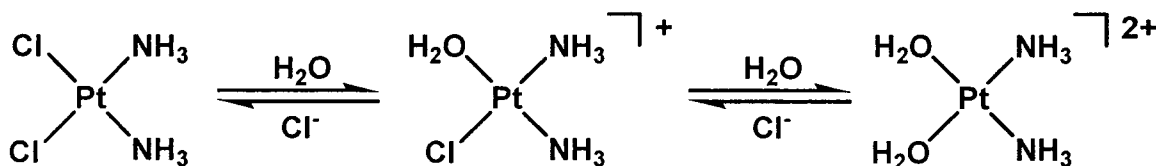
Scheme 1. Aquation of cisplatin.

Thus, cisplatin is, in essence, a pro-drug with active species being generated *in vivo*. Once aquation occurs inside the cell, the labile aqua ligands may be replaced by donor atoms on biomolecular sites including the N7 of the purine bases of DNA [6]. Indeed, it has been observed that the chelation of 2/3 of all platinum occurs at the N7 of adjacent guanine residues forming a bifunctional adduct [6]. Although it is possible for cisplatin to bind to DNA at other sites, such as adenine, these interactions are less frequent [4].

The result of DNA chelation on the conformation of the biomolecule is undoubtedly substantial. Crystallographic studies have shown that platination

causes a bend in the DNA structure 30-55° towards the platinum centre located in the DNA major groove in addition to unwinding of the base pairs [6]. The DNA damage induced by cisplatin promotes the binding of nuclear high-mobility group (HMG) proteins to the lesions [5]. The specific role of HMG proteins in the cellular response to platinated DNA remains obscure, and results remain inconclusive as to whether these proteins are involved in the protection of the lesion or in the promotion of DNA repair [6]. However, in some instances, cell death will occur via apoptosis and in others DNA repair may result in survival [6], depending on the extent of DNA damage and the cells that were exposed.

A mass of information regarding the complex nature of the cellular responses to cisplatin has surfaced over the years; however, these specific details are above and beyond the scope of this project. Nevertheless, the functional ambiguity of the HMG proteins is far from the solitary mystery surrounding biological responses to cisplatin [5]. Questions regarding the remarkable activity of cisplatin still remain including, among others, why the efficacy of this compound was not observed for certain types of malignancies (eg. breast and prostate tumours) [5]. Although it has been in clinical practice for more than 30 years, there are many aspects regarding the biological effects of cisplatin that remain to be elucidated. The mysteries surrounding cisplatin remain intriguing and, still to this day, attract a great deal of research initiatives. The illumination of these shaded facets, pertaining to the specific mode of action of this pivotal chemotherapeutic agent, is certain to aid in the design and administration of future metal-based anticancer compounds.

1.3 General Limitations of Cisplatin

Although cisplatin remains an important chemotherapeutic agent, there continue to be several major problems and disadvantages that may be associated with its use. One issue pertaining to the clinical administration of cisplatin is that it invokes a number of adverse side effects resulting from its nonspecific general cytotoxic properties. These maladies include nephrotoxicity, neurotoxicity, vomiting, and nausea [4,7]. However, co-administration of other medications and hydration therapy can alleviate the side effects to make the treatment more tolerable for the patient [4,7].

Another issue regarding the use of cisplatin concerns the inherent resistance to this compound that some tumour cells possess. Despite the fact that cisplatin is active against many types of cancers, there are a number of common malignancies that display an innate resistance to the treatment including lung, breast, prostate and colorectal cancers [3,4]. Furthermore, cisplatin is inactive against many secondary tumours [8]. Unfortunately, other means of treatment must be followed in order to manage these diseases.

Not only are some cells inherently resistant to cisplatin chemotherapy but tumours may also acquire cisplatin resistance after primary treatment, presenting a significant clinical problem. Although levels of resistance less than 50-fold are most common, extreme cases of 1000-fold resistance have been reported [9]. In fact, even small levels of resistance can be clinically significant. Tumours that

acquire resistance are no longer susceptible to the chemotherapeutic effects of cisplatin at the original dosage [9]. Thus, to continue cisplatin treatment, dosages must be increased risking severe toxic effects that may include: neuropathy, kidney and bone marrow failure, excessive vomiting, blindness, deafness and seizures [9]. These symptoms echo the fact that cisplatin is a general cytotoxin capable of affecting many types of tissues.

In light of the multifactorial and complex mode of action of cisplatin, it may not be surprising that the cause of the cellular resistance to this drug may be attributed to a combination of several cellular mechanisms [10]. The specific mechanisms, and the degree to which they are involved, seem to be dependent on the type of malignant cells. One possible mechanism of cisplatin resistance involves decreased intracellular accumulation of the drug (i.e. pharmacokinetics). This effect may be an individual or combined result of decreased cellular uptake and increased efflux of cisplatin [10]. It is well understood that clearance rates of drugs from the body vary between individuals within a population, and can also vary with age, health and body status. There is also increasing number of studies showing that personal genomics and ethnicity play a major role in efficacies of drugs, making pharmacogenomics an increasingly important consideration in the administration of drugs.

Another postulated mechanism of cisplatin resistance revolves around an increase in the intracellular levels of thiol-containing molecules. Cytoplasmic components such as glutathione and metallothionein contain nucleophilic cysteine residues that bind and inactivate cisplatin as a result of ligand

substitution involving the labile aqua ligands and the thiol functionalities of these compounds [9,10]. Upregulation of these thiol-containing molecules enables the cell to disable the aquated cisplatin species before DNA damage can occur.

Evasion of the apoptotic consequences of cisplatin is not limited to mechanisms of interception that take place before the metallodrug has had an opportunity to interact with DNA. In fact, resistance may also transpire at this primary site of action. In order to avoid cell cycle arrest and apoptosis once the cisplatin-DNA adducts have formed, cells may employ a nucleotide excision repair mechanism [9,10]. This system relies on a network of proteins that concert the removal and replacement of the damaged DNA fragment. Cells that are deficient in nucleotide excision repair exhibit increased cisplatin sensitivity, and restoring this functionality re-establishes sensitivity to normal levels [10].

Although it has secured its place in the clinic and has proven to be an astounding pharmaceutical, the problems associated with cisplatin remain as substantial clinical challenges. These issues have promoted the search for alternative compounds that display novel anticancer properties and improve upon the medical complications associated with cisplatin.

1.4 Derivatives of Cisplatin: Carboplatin and Oxaliplatin

Naturally, with the advent of cisplatin came a surge in research focusing on the design, synthesis and testing of other structurally similar platinum compounds that demonstrate antiproliferative properties [4,8]. Unfortunately, only

a small fraction of the thousands of compounds that were screened achieved

entrance into clinical trials. Only two platinum anticancer compounds have since

been approved for worldwide clinical use, namely carboplatin and oxaliplatin

(Figure 2) [4,8].

The molecular structure of carboplatin is very similar to that of cisplatin in

that it is a square planar platinum(II) compound containing two *cis* ammine

ligands; however, the chloride leaving groups have been substituted for a

chelating dicarboxylate ligand. Despite this structural change, carboplatin is

active against the same spectrum of cancers, and is believed to have a parallel

mode of action as compared to cisplatin [4]. Interestingly, the benefit of

carboplatin is the lack of severity with respect to side effects [4,6].
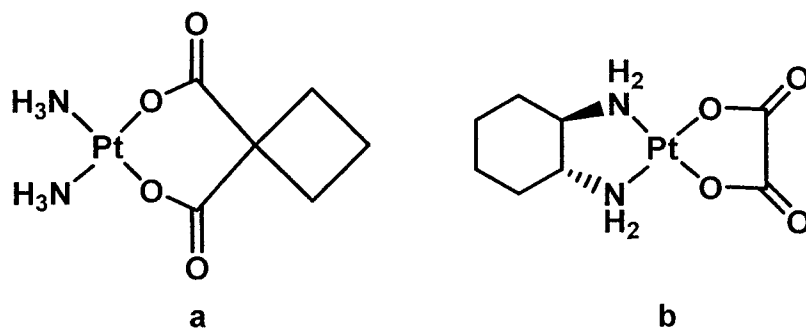
Figure 2. Molecular structures of: (a) carboplatin and (b) oxaliplatin [4].

The differing toxicological profile of this platinum compound allows for the

administration of higher doses compared to cisplatin, and is the factor that

propelled its introduction to worldwide use [4]. This improvement is a result of the

incorporation of the less labile (compared to chloride) chelating dicarboxylate

group allowing for fewer biomolecular interactions with carboplatin. However,

because of this change of leaving group, carboplatin has a rate of aquation two orders of magnitude lower than that of cisplatin, and is, therefore, slightly less active against most malignancies [4,7]. Furthermore, as might be expected from the analogous mode of action, carboplatin has shown cisplatin cross-resistance [7]. Therefore, cisplatin remains the preferred treatment compared to carboplatin with the latter being used when the side effects of cisplatin are an issue due to other medical complications [4].

The third platinum compound that has been approved for worldwide clinical use is oxaliplatin. The chemical structure of this compound is once again similar to that of cisplatin except that the chlorides are replaced with a bidentate oxalate ligand and the ammines are replaced by a chelating 1,2-diaminocyclohexane (dach) ligand [11]. The advantage of oxaliplatin lies in the range of cancers that are treatable by this compound. Although it is active against the same malignancies as cisplatin and carboplatin, oxaliplatin is effective in the treatment of colorectal cancer [12] in addition to some cisplatin resistant cancers [4].

Oxaliplatin forms similar DNA adducts as those of cisplatin and carboplatin except that the active platinum component of oxaliplatin contains the dach moiety [13]. It is this structural variation that is believed to widen its spectrum of activity to include colorectal cancers and various cisplatin resistant strains [4]. Although the role that the dach ligand plays in the activity of the compound has yet to be fully clarified [4], it has been suggested that the difference in the DNA conformational change produced by oxaliplatin as

compared to cisplatin-DNA adducts and the hydrophobic properties of the dach ligand may aid in circumventing the detection of oxaliplatin-DNA lesions by the proteins involved in the DNA repair mechanism [13].

The approval of carboplatin and oxaliplatin for worldwide utilization provided the option for treatment with less severe side effects than cisplatin and the inclusion of colorectal and cisplatin resistant cancers into the array of malignancies that are treatable by platinum-based compounds. However, it was clear that, in order to design compounds that could exceed cisplatin and its derivatives in their faults and limitations, it would be necessary to break the design mold and explore compounds that defy the structure-activity relationships that have emerged from experimentation with these types of platinum compounds.

1.5 Alternative Metals: Gold-Phosphine Anticancer Complexes

One novel approach to the design of anticancer compounds is the use of metal ions other than platinum in the molecular scaffold. Over the years, there have been a multitude of compounds based on alternative metals investigated for antiproliferative properties [1,4,14]. Furthermore, the ligand systems that have been applied in these studies are seemingly endless and have proved to play an important role with respect to the compounds' activity. A particularly interesting subset of compounds that have received a great deal of attention with respect to their antiproliferative effects are gold-phosphine compounds [14].

Interestingly, auranofin was among the primary gold-phosphine complexes that were shown to have anticancer properties. Auranofin (Figure 3), a linear gold(I) compound containing a tetraacetylthioglucose ligand and a triethylphosphine ligand, is used in the treatment of rheumatoid arthritis [15]. The gold complex was shown to have promising therapeutic results when tested in mice bearing P388 lymphocytic leukemia; however, further investigation revealed that the compound had a limited spectrum of activity with respect to other murine tumour models *in vivo* [16]. Nevertheless, the anticancer activity of auranofin was intriguing and inspired investigations into the mode of action of this complex.
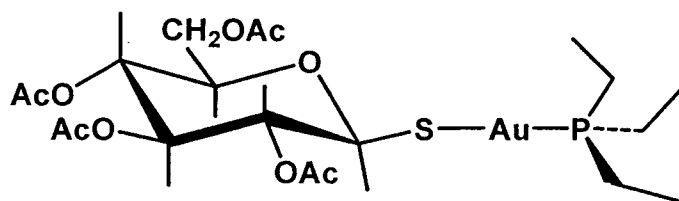
Figure 3. Molecular structure of auranofin [16].

Early evidence showed that *in vitro* cellular response to auranofin was characterized by extensive morphological changes and non-selective inhibition of DNA, RNA and protein sysntheses as exhibited at high drug concentrations within a short period of time [17]. Conversely, DNA binding studies suggested that interaction with DNA was not the likely cause of anticancer activity of this compound due to the lack of reactivity of this drug with DNA *in vitro* [17]. Recent studies suggest that the antitumour activity of auranofin may be via induction of

apoptosis resulting from its inhibitory effects on mitochondrial thioredoxin reductase rather than DNA interaction [18].

An auranofin derivative that contains a chloride ligand in place of the tetracetylthioglucose ligand has also shown antiproliferative activity. Although this structural change reduces the antitumour activity *in vivo* relative to auranofin, (Et$_3$P)AuCl is highly cytotoxic *in vitro* [17,19]. Early investigations regarding the mode of action of this complex revealed that mitochondrial levels of NADPH, NADH, and ATP were reduced after only a brief exposure to the gold compound suggesting that this organelle and oxidative phosphorylation may be initial targets [17]. Like auranofin, (Et$_3$P)AuCl has been shown to interact with thioredoxin reductase, and the induction of apoptosis due to this interruption of the thiol redox balance is also a possibility [18].

Another gold(I) phosphine compound that received much attention due to its anticancer properties was the tetrahedral [Au(dppe)$_2$]Cl complex (where dppe is 1,2-bis(diphenylphosphino)ethane) reported by Sadler and coworkers (Figure 4) [20]. Amazingly, the cytotoxicity of this coordination complex was comparable to cisplatin in a number of cancer cell lines [14]. Although there is evidence that [Au(dppe)$_2$]Cl induces apoptosis by a mitochondrial mechanism, it likely functions in a different manor than that of auranofin and (Et$_3$P)AuCl due to the fact that it does not readily react with thiols [19,21]. DNA-protein cross-links have been observed in cells that have been exposed to [Au(dppe)$_2$]Cl. In addition, this complex has shown the ability to produce DNA strand breaks, but
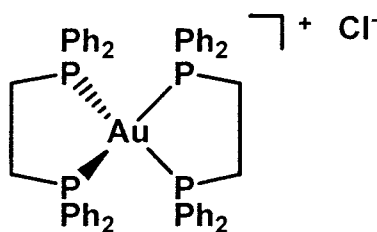
Figure 4. Molecular structure of [Au(dppe)$_2$]Cl [14].

only at concentrations above which are required for cell lethality [14].

Unfortunately, this compound proved to induce severe liver damage in canine

models under the scrutiny of pre-clinical trials, and therefore, the trials were

abandoned [18].

A number of compounds structurally similar to [Au(dppe)$_2$]Cl have been

screened for their antiproliferative effects exposing structure-activity relationships

[21]. It was discovered that, for complexes of the general formula [Au(R$_2$P(CH$_2$)$_n$

PR'$_2$)$_2$]X, the most active species were those that had phenyl substituents on the

phosphines and where n= 2 or 3, or the phosphine bridge was composed of an

ethylene group in a *cis* configuration [21]. Interestingly, substitution of the phenyl

moieties by other groups generally decreases the activity of the compound or

renders it inactive [18,21]. However, recent work by Berners-Price and coworkers

has shown that it is posible to induce selectivity for cancer cells by tuning the

hydrophilic/lipophilic nature of these complexes using pyridyl phosphine analogs

of the dppe ligand in the structure of these gold compounds [18]. Interestingly,

activity was maintained when gold was substituted for silver(I) or copper(I), but

lost activity with respect to the analogous palladium(II) and platinum(II)

compounds [18]. This implies that the mode of action of these complexes

depends not only on the ligands present but also on the identity of the metal. For example, DNA is the suspected target of a variety of copper(I) dppe complexes inducing cell cycle arrest and apoptosis [22].

The large body of experimentation concerning gold-phosphine compounds and their antitumour potential has greatly advanced the field of metal-based chemotherapeutics. Interestingly, the National Cancer Institute has screened a wide range of metallophosphines for anticancer properties and has generally found them inactive; however, Sadler and Berners-Price have suggested that these complexes should be reevaluated based on the small range of cancers used in these studies and the conditions under which they were tested [14]. Conversely, it has become clear from various studies involving metal-based phosphine compounds that they possess the potential to be important anticancer chemotherapies, and exploration of various phosphine ligands along with the identity of the metal will be crucial in their development.

1.6 Introduction to Ruthenium Anticancer Compounds

Some of the most exciting results that have astonished the field of metal-based chemotherapy have been the anticancer activity of novel ruthenium complexes. Although it has been known for decades that ruthenium ammino complexes display anticancer properties [1], only recently has the true capacity of ruthenium anticancer compounds begun to surface. While the rapid discovery and expansion of potential ruthenium antitumour compounds is ongoing, two

fascinating classes of compounds have emerged. The first class contains the octahedral anionic ruthenium(III) compounds NAMI-A and KP1019 [4]; whereas the second set is composed of the ruthenium(II) RAPTA-type complexes developed by Dyson and the ruthenium(II)-arene complexes developed by Sadler (*vide infra*) [4].

One property of ruthenium compounds which might make them suitable in anticancer applications is their potential to utilize the natural iron transport system to accumulate in cells [1]. This ability imparts a degree of specificity with regard to the targeting of cancerous cells as opposed to normal tissue. The uncontrolled growth of malignant cells bestows a greater need for metabolites such as iron compared to normal cells; the receptors for transferrin, a serum protein that transports iron into the cell, are overexpressed in many solid tumours [23,24]. In addition, the increased energy needs of tumour cells increases the formation of new blood vessels (angiogenesis) at the tumour site providing better access to metabolites and, consequently, transferrin [1]. Thus, the ability of ruthenium complexes to bind to transferrin offers a method for these compounds to become preferentially sequestered in malignant tumour cells.

1.7 Ruthenium(III) anticancer complexes

An interesting postulation made by Clarke regarding the activity of the ruthenium(III) compounds is a concept that has become known as the "activation by reduction" hypothesis [1]. Ruthenium(III) compounds are, in general,

substitutionally inert and, therefore, relatively nontoxic [23,25]. These complexes may be reduced selectively in cancer cells to the more reactive ruthenium(II) species due to the different metabolic conditions inside tumours. These conditions include a lower pH resulting from the accumulation of lactic acid generated from glycolysis and a decreased molecular oxygen concentration that arises due to increased metabolic requirements of cancerous cells [1]. This is because the major glycolytic pathway employed by cancer cells to generate ATP is anaerobic, bypassing the Citric Acid Cycle and electron transport chain in the mitochondria, leading to the increased lactic acid production. Not only would the lower electrochemical potential generated by these abnormal metabolic conditions favour the production of ruthenium(II), but also redox proteins such as glutathione are capable of reducing ruthenium(III) compounds in the cell [1].

NAMI-A, the first ruthenium anticancer complex to enter clinical trials, is a ruthenium(III) compound with four chloride ligands situated in a meridional geometry, an imidazole *trans* to a sulfur-coordinated dimethylsulfoxide ligand, and imadozolium as a counter ion (Figure 5) [4]. Developed by the groups of Alessio and Sava, the antitumour characteristics of this compound were discovered in the early 1990s [26], and over the years it has shown some very surprising antitumour activity. Although NAMI-A is relatively non-toxic to primary tumours, it has shown remarkable activity with respect to metastases of solid tumours [4]. Metastasis is the process by which tumour cells disperse and form secondary tumour deposits in other locations in the host [27]. Compounds that display antimetastatic activity are truly extraordinary due to the devastating

16

clinical problems that are associated with metastasizing cancers. Unfortunately, metastatic cancers are often resistant to standard therapies and it is estimated that an astounding 90% of cancer deaths are a consequence of metastasis [27]. Thus, the importance of the development of antimetastatic agents cannot be over emphasized.
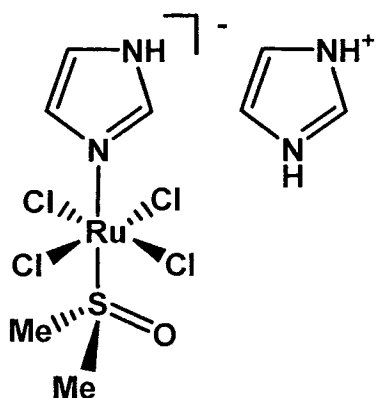
Figure 5. Molecular structure of NAMI-A, an antimetastatic ruthenium(III) compound [4].

Although the specific mode of action of NAMI-A has yet to be determined [28], a wealth of information has been amassed regarding its chemical and biological activity. Under physiological conditions NAMI-A undergoes hydrolysis, producing a mixture of aquated species [29]. The interactions of the ruthenium complex with DNA are weak, and it is suspected that the activity of NAMI-A is a consequence of its interactions with proteins [28,30]. Indeed, the drug may function by disturbing processes such as cytoskeletal rearrangement, motility, gelatinase functionality, and angiogenesis all of which play a role in tumour invasion [28]. It has been demonstrated that NAMI-A inhibits a variety of matrix metalloproteinase enzymes that are involved in the decomposition of the

extracellular matrix, and have been linked to tumour growth, invasion and metastases [28]. Furthermore, interaction with membrane surface proteins may also contribute to the molecular mechanism of this compound [4].

A few years ago NAMI-A was evaluated in phase I clinical trials aimed at the determination of the maximum tolerated dose, profile of adverse effects, and dose-limiting toxicity in human cancer patients [31]. These studies revealed that NAMI-A was generally well tolerated in humans; however, a dose-limiting response of blister formation was observed as well as nausea and vomiting, which could be controlled with the use of other medications [31]. Renal dysfunction was also observed, but was reversible [31]. Nevertheless, it was suggested by the authors that NAMI-A should enter phase II clinical trials to continue with the investigation of this drug in a clinical setting.

Another compound, developed by Keppler, which has received a great deal of attention, is KP1019. This compound is composed of a ruthenium(III) centre with two indazole ligands in a *trans* configuration with four chloride ligands completing the coordination sphere and an indazolium as a counter ion (Figure 6) [4]. Although KP1019 is structurally similar to NAMI-A, their anticancer properties differ substantially.

KP1019 has shown cytotoxic properties against a variety of tumour models both *in vitro* and *in vivo*. Most significant is the cytotoxic activity of KP1019 when tested in cisplatin resistant tumour models and colorectal cancers [4,32]. Hydrolysis products of KP1019 are formed under physiological conditions and it is believed that the drug enters the cell by binding to transferrin [32]. Once

inside the cell, the evidence suggests that the hydrolysis compounds are likely to undergo activation by reduction producing reactive ruthenium(II) compounds inside the malignant cells [4,33]. These mechanisms may explain the low general toxicity of KP1019. While DNA is the suspected biochemical target of this
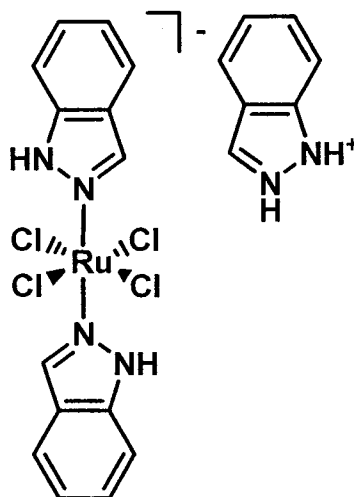
Figure 6. Molecular structure of the ruthenium(III) anticancer compound KP1019 [4].

complex, there is indication that the lesions produced are processed differently by the cell compared to those produced by cisplatin [33]. This explains the activity of KP1019 against colorectal cancers and cisplatin resistant cells. Furthermore, since the exact mode of action is unknown, mechanisms involving binding of KP1019 to proteinaceous histidine residues should not be ruled out [4].

Recently, KP1019 has been subjected to phase I clinical trials. Amazingly, no side effects were observed in these studies and stablization of diseases were achieved in five of the six patients participating in the study. In light of these exciting results, the outcomes of phase II clinical trials of KP1019, (i.e. evaluating

the therapeutic potential of this complex) are greatly anticipated and should prove to be rather intriguing.

1.8 Ruthenium(II) anticancer complexes

Although ruthenium(III) complexes may utilize the activation by reduction pathway in their anticancer mechanisms, a number of ruthenium(II) compounds that are already in a reduced state have shown amazing anticancer properties. Two such classes of prospective metallopharmaceuticals are the RAPTA-type (Ruthenium Arene PTA complexes, where PTA= 1,3,5-triaza-7-phosphaadamantane and its derivatives) complexes and the Sadler-type complexes. With striking similarity to NAMI-A and KP10191, these two types of compounds display exceptionally different anticancer properties despite their structural resemblance.

1.9 RAPTA-type Anticancer Complexes

The prototypical molecular structure of the series of RAPTA compounds can be described as a ruthenium(II) centre with a facially bound arene ligand in a *trans* configuration with respect to a PTA ligand and two chlorido ligands (Figure 7) [4] . These types of structures are commonly referred to as "piano stool" complexes due to their resemblance to these furnishings with the arene moiety as the "seat" of the stool and the ancillary ligands reminiscent of the stools "legs".

Similar to NAMI-A, RAPTA complexes do not display activity against primary tumours but are selectively active against metastases [34]. A great deal of ligand variation has been used in experimentation with the RAPTA complexes in order to establish structure-activity relationships.
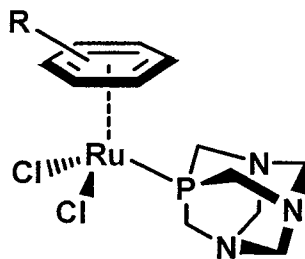
Figure 7. General molecular structure of the antimetastatic RAPTA-type compounds [4].

An early theory explaining the mode of action of these complexes involved the protonation of one of the nitrogens of the PTA ligand. It has been shown that the protonation of the PTA ligand occurs at reduced pH [35]. It was believed that the result of this protonation was two-fold: to trap the complex inside the cell and also to cause damage to DNA [36]. The selectivity would be induced by the fact that the protonation of the RAPTA complex would only occur in the reduced pH environment found in cancerous cells, and that protonation was a requirement for the compounds to cause DNA damage [36].

Although DNA damage may be a contributing factor, it is currently believed that DNA is not the solitary biomolecular target of RAPTA compounds [37]. A great deal of information regarding the cellular response to the most promising candidate of this series of compounds, RAPTA-C (where the identity of

the arene in the general structure is *p*-cymene), has been elucidated and can be summarized as follows [38]:

- G2/M phase cell cycle arrest and the induction of apoptosis is associated with the exposure to RAPTA-C resulting in prolonged survival is mice.

- The G2/M phase cell cycle arrest is associated with the escalation of p21 expression in a p53-dependant fashion and the decreased levels of cyclin E.

- The administration of RAPTA-C was associated with the increase of cytochrome *c* levels activating procaspase-9, therefore, resulting in the promotion of apoptosis.

- RAPTA-C caused the inhibition of cell growth mediated by activation of c-Jun NH_2-terminal kinase and stabilization of p53.

Indeed, these recent *in vivo* studies reveal that the mechanistic activity of RAPTA-C is complex, and is a result of multiple apoptotic and cell cycle arrest pathways [38]. The involvement of multiple pathways in the activity of RAPTA may reduce the development of drug resistance in response to this type of compound [38]. The hydrolysis of RAPTA-type compounds has been studied, and it has been established that a variety of aquated species may form under physiological conditions, which may be crucial in their interaction with molecular targets [39]. Furthermore, RAPTA complexes can bind to proteins to form stable

adducts [40] and significant inhibition of cathepsin B has recently been observed by a variety of these compounds [41]. Capthesin B is an enzyme capable of the degradation of components in the extracellular matrix and is believed to play an integral role in metastasis, angiogenesis and tumour progression [42]. These types of interactions may be integral in their modes of action pertaining to the RAPTA complexes.

In an attempt to elucidate structure-activity relationships, a great deal of ligand variation has been employed in the RAPTA framework. For example, RAPTA-C analogues that replace the chloride ligands with a bidentate oxalate ligand (oxaloRAPTA) or cyclobutane dicarboxylate ligand (carboRAPTA) were synthesized (Figure 8) [43]. The purpose of this modification was to reduce hydrolysis and determine if this had an effect on anticancer activity. Although the

a   b
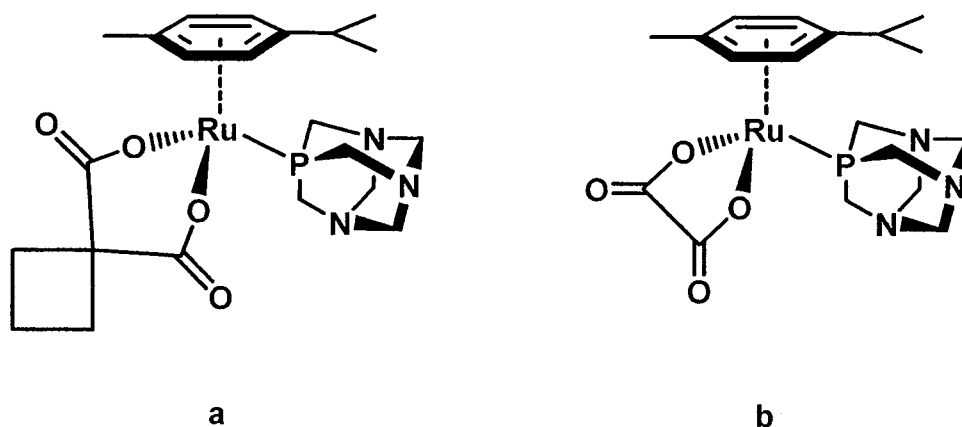
Figure 8. Molecular structures of: (a) carboRAPTA and (b) oxaloRAPTA, complexes that resist hydrolysis [43].

complexes containing the bidentate leaving groups did not undergo aquation as readily as RAPTA-C, they seemed to have remarkably similar *in vitro* activities against cancer cell lines [41]. However, since the innovative nature of RAPTA-C lies in its ability to reduce metastases, it is unclear if these analogues are beneficial compared to the parent complex with respect to their activity against these types of cancers based on these studies. Evidence for the necessity of chloride substitution in the activity of these compounds was discovered in the study of a wide range of RAPTA analogues and their abilities to inhibit cathepsin B. It was found that the ability to inhibit this enzyme was dramatically reduced for the analogues containing the bidentate oxalato or dicarboxylato leaving groups [41]. This suggests that chloride substitution is required for the interaction of RAPTA complexes and cathepsin B. Furthermore, these studies revealed that the identity of the arene is important towards interactions with this biomolecule. The steric bulk of the arene seems to have a negative impact on the inhibition of cathepsin B by RAPTA compounds [41]. The steric restraints, imposed by larger arene ligands, may hinder the interaction of RAPTA complexes and the active site of the enzyme.

These experiments have revealed interesting clues regarding the biomolecular targets of these potential metallodrugs and the cellular responses that they stimulate. With the advancement of these novel RAPTA compounds, new targets for future metal-based antitumour compounds are certain to be exposed.

1.10 Sadler-type Piano Stool Complexes

Another fascinating group of anticancer compounds that has received a great deal of attention recently is the Sadler-type piano stool complexes. The exemplary structure of these compounds follows the piano stool scaffold consisting of a ruthenium(II) centre with a face-capping arene ligand. The three remaining coordination sites are occupied by a chlorido ligand and a chelating bidentate ligand (Figure 9) [23]. A number of these types of compounds have shown amazing anticancer properties, both *in vitro* and *in vivo*, and a wealth of information regarding their mode of action has emerged. As with the RAPTA complexes, many structure-activity relationships have also been established for these piano stool compounds.
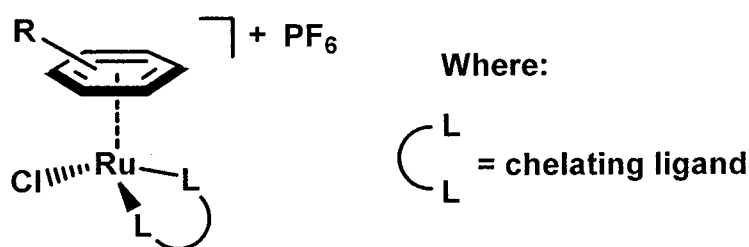
Figure 9. General molecular structure of the Sadler-type complexes [25].

The Sadler-type compounds display a wide range antiproliferative activity. Although DNA is the molecular target of these compounds, the adducts that are formed by the interaction of these ruthenium(II) compounds with DNA are significantly different from those formed by cisplatin. This has been illustrated by the fact that these compounds have been shown to be equally as effective

25

towards wild-type and cisplatin-resistant human ovarian cancer cells *in vitro* [25,44]. Under physiological conditions, the Sadler-type compounds are hydrolyzed to form the mono-aquated species [45]. As with the other compounds discussed, this process is thought to be favoured intracellularly due to the reduced chloride concentrations as compared with extracellular chloride concentrations [46]. The complexes preferentially bind to the N7 of guanine bases on the DNA target via covalent interaction with the ruthenium(II) centre [25]. Adenine may also be a site of interaction depending on the choice of chelating ligand present in the piano stool complex. Further stabilizing the DNA adduct are the possible interactions of the arene and chelating ligands with the biomolecule. The arene moiety has been shown to interact with nucleobases in a π-stacking manner suggesting that these structures may insert into the DNA framework adding stability to the metallodrug-DNA adduct [47]. Furthermore, groups on the chelating ligand may form strong electrostatic interactions with exocyclic functionalities (amine or carbonyl) of the purine bases [47]. The accumulation of these interactions can be quite significant; their optimization can result in remarkable anticancer activity [48].

A number of Sadler-type analogues have been synthesized and screened for their anticancer properties, and from these studies a number of structure-activity relationships have become apparent. Indeed, the structure-activity relationships that have emerged can be explained on the basis of the interaction of the compound with the DNA target as described above. For example, results have shown that the antiproliferative activity of these complexes generally

increases with the size of the arene moiety. The following general activity trend

has been observed [48]:

benzene < *p*-cymene < biphenyl < dihydroanthracene < tetrahydroanthracene

Hence, the greatest activity of these compounds tends to be observed for those

that contain polycyclic aromatic hydrocarbons. The greater activity with increased

size of the arene is likely due to the enhanced intercalative abilities of these

extended arene groups [48]. In addition, the larger more hydrophobic arenes may

facilitate cellular uptake of the piano stool complex, and promote DNA interaction

through hydrophobic interactions [25].

Variation of the chelating ligand has also given rise to a number of

structure-activity relationships. As previously mentioned, the identity of this ligand

can affect the nucleobase specificity of these compounds. It has been

demonstrated that the presence of an amine-donating group on the chelating

ligand can have strong hydrogen bond interactions between the amino

hydrogens and the exocyclic oxygen of the guanine nucleobase; however,

repulsive interactions are observed between the amino hydrogens of the

chelating ligand and the exocyclic amino hydrogens of the adenine nucleobase

[49]. The presence of the amino hydrogens is crucial and can be exemplified by

the fact that the use of 2,2'-bipyridine (bipy) or N,N,N',N'-tetramethylenediamine

(tmeda) as the chelating ligand yields complexes with insignificant

antiproliferative activity; whereas, incorporation of ethylenediamine (en) or 1,2-

diaminobenzene (dab) into the molecular design afford complexes with

remarkable activity (Figure 10) [48]. Amazingly, some of the most active Sadler-type complexes that have polycyclic arene moieties and chelating ligands capable of the hydrogen bonding interaction described above display activity comparable to those of carboplatin and cisplatin in the A2780 human ovarian cancer cell line [44].
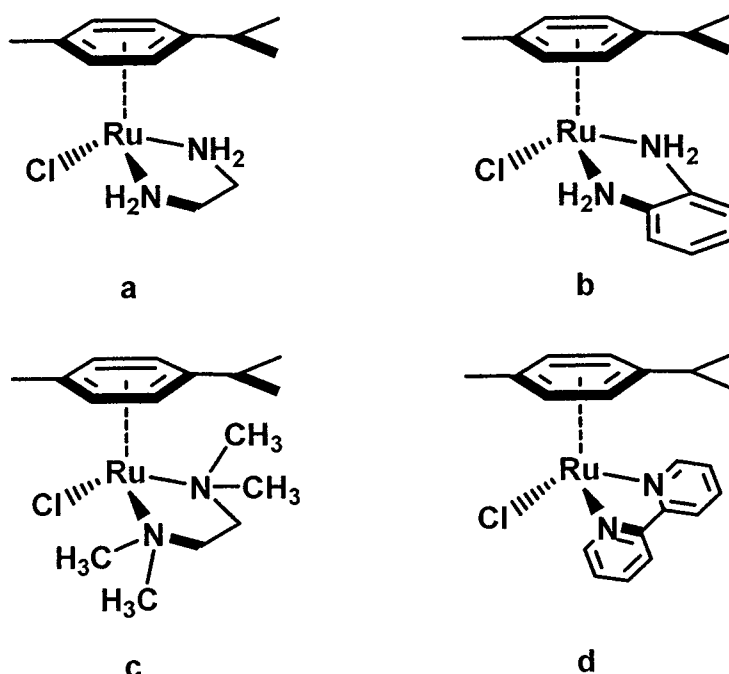
Figure 10. Variation of the bidentate ligand system in Sadler-type compounds with *p*-cymene as the arene: (a) en and (b) dab have amino hydrogens and are cytotoxic; whereas, (c) tmeda (d) bipy are inactive [48].

The use of a chelate ligand containing oxygen donor atoms such as acetylacetonate (acac) makes the binding affinities of these compounds toward the N7 of guanine and adenine similar [50]. The ability of the oxygen atoms of the acetylacetonate ligand to engage in hydrogen bonding interactions with the exocyclic amino hydrogens of adenine is likely the cause of this increased affinity

28

of these compounds for this DNA component [51]. Crystallographic and computational data have provided evidence of the interaction of these chelating ligands with the C6 exocyclic moieties of purine bases as illustrated in Figure 11 [49,51,52].
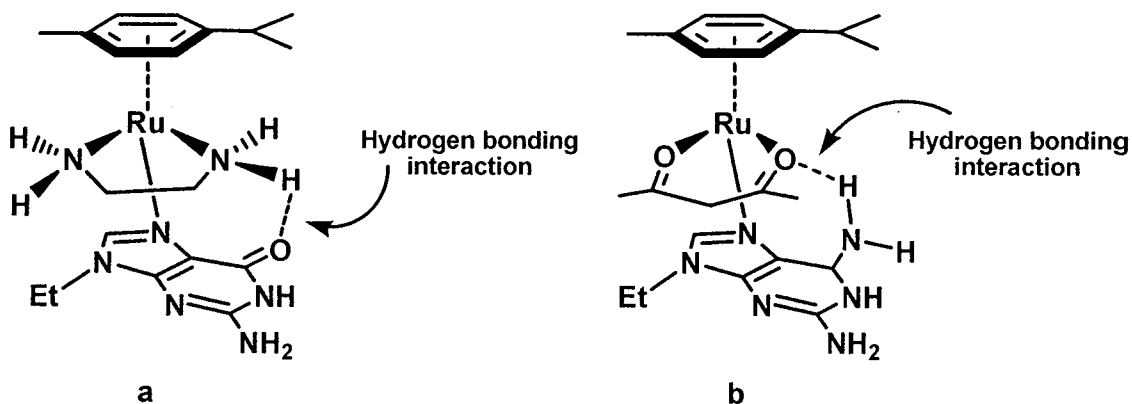
Figure 11. Hydrogen-bonding interactions between Sadler-type compounds and model DNA bases: (a) en complex and 9-ethylguanine; (b) acac complex and 9-ethyladenine [49,51,52].

Further demonstrating the necessity for aquation in the activity of Sadler-type anticancer compounds are the structure-activity relationships that arise due to variation in the leaving group. It has been shown that these complexes can have rates of hydrolysis spanning many orders of magnitude, and that this can have a dramatic effect on the activity of the complex [25]. In general, complexes that aquate (i.e. where the leaving group is halide, azide or dichloropyridine) are active in the A2780 human ovarian cell line, whereas complexes that do not aquate (i.e. where the leaving group is pyridine) are inactive [53]. Thus, the lability of the leaving groups plays an integral role in the activity of these complexes.

29

Nevertheless, these structure-activity relationships are not as sharply defined as they may seem. In fact, antiproliferative activity increases with the incorporation of smaller arene ligands in systems that employ acetoacetonate as the bidentate ligand - a trend that is in opposition to the structure-activity relationship observed in other Sadler-type complexes. In addition, complexes that have thiophenolate as leaving groups are not easily hydrolyzed, and their antiproliferative activity is thought to arise from their activation by another mechanism [53]. These studies reverberate the notion that the variation of the leaving group of these piano stool compounds is another method by which the activity of these complexes may be tuned.

1.11 Ruthenium-Cyclopentadienyl Phosphine Anticancer Compounds

A new class of highly active anticancer compounds that appeared in the literature as this project was culminating deserves special mention due to the fact that they are closely related to the compounds resulting from this work. A pair of ruthenium(II) compounds (Figure 12) with the configuration [(η^5-C_5H_5)Ru(L)(PP)][CF$_3$SO$_3$] (PP= 1,2-bis(diphenylphosphino)ethane, L= 1,3,5-triazine; PP= 2 triphenylphosphine, L= pyridazine) were recently shown to possess potent antiproliferative activity *in vitro* [54]. The complex containing the triphenylphosphine ligands was slightly more potent in the cell lines tested, and it was suspected that the two compounds had differing modes of action.

In the case of the diphosphine compounds, it was found that substitution

of this ligand did not occur and DNA intercalation of the aromatic rings was

suspected. Conversely, at least one of the triphenylphosphines was found to be
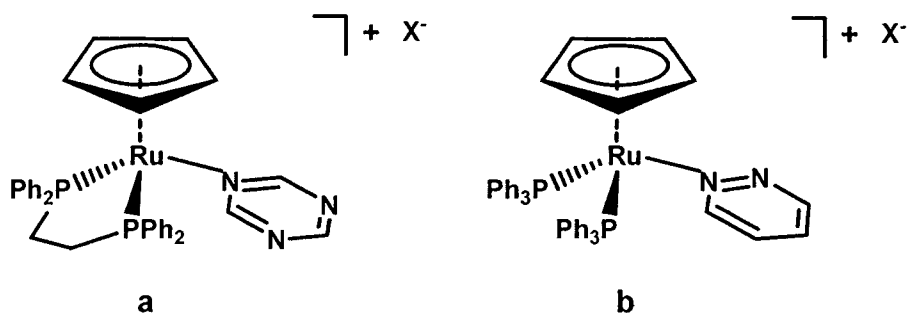
Where X⁻ is CF₃SO₃⁻

Figure 12. Ruthenium(II)-phosphine anticancer compounds containing: (a) dppe and

1,3,5 triazine, (b) triphenylphosphine and pyridazine [54].

displaced by a dimethylsulfoxide ligand and subsequently with a nitrogen from a

purine base [54]. These intercalative and covalent interactions were supported by

changes in free plasmid DNA as observed using atomic force microscopy [54].

This study is the first of an emerging class of potent ruthenium(II)-

phosphine anticancer agents. Although these preliminary results describing their

antiproliferative effects are rather astounding, explications of the pharmacological

properties of these complexes will also prove to be interesting.

The extraordinary and promising anticancer activity of ruthenium-based

compounds is very exciting with regard to expanding the spectrum of treatable

malignancies by metallopharmaceuticals. The remarkable ability of NAMI-A and

the RAPTA complexes to reduce the formation of metastases may prove to be a

giant leap forward in the treatment of cancer due to the giant clinical challenges that secondary tumours pose. In addition, the potent activity and low general toxicity of KP1019 and the Sadler-type compounds, along with their ability to treat cisplatin-resistant cancers, add tremendously to the importance of the research and development of novel ruthenium anticancer compounds. It may be in the near future that ruthenium complexes will provide clinicians the means to treat such devastating malignancies. Moreover, the recent discovery of ruthenium(II)-phosphine compounds that display antiproliferative effects is indicative of the emergence of a new class of anticancer compound that may prove to be powerful antitumour complexes. The ability to easily fine-tune these coordination compounds in order to elicit structure-activity relationships and to manipulate their bioactivity adds to their attractiveness as anticancer treatments [55].

1.12 Determination of Cytotoxicity Via the MTT Assay

The 3-{4,5-dimethylthiazol-2-yl)-2,5-diphenyltetrazolium bromide (MTT) assay has become a commonly used test for screening the cytotoxic effects of potential anticancer compounds. This colourimetric method is beneficial in that it is a very reproducible, quick and relatively simple method to screen many compounds simultaneously for antiproliferative effects [56].

The assay measures the amount of formazan (purple) that is present in living cells due to the reduction of MTT (yellow) by mitochondrial dehydogenase activity [58] that is absent in dead cells [57]. Therefore, the MTT assay is an

indirect measure of cell viability. However, one must be careful when interpreting the results obtained from MTT assays. Although it is an extremely useful *in vitro* screening method for cytotoxic agents, compounds that are selective towards metastases may not produce significant IC_{50} concentrations as in the case of NAMI-A and the RAPTA complexes and will require other methods to assay for activities. Such compounds would slip through a screening process solely based on the MTT assay, and their true activity may not be realized.

2. Research Intentions and Rationale

The tris(pyrazolyl)borato ligand class has been one of the most extensively studied ligand architectures in coordination chemistry since its inception in the 1960s [59]. Its sister ligand class, tris(pyrazolyl)methane (tpm) and its derivatives, have not been explored as much due to its history of being plagued with difficulties pertaining to its synthesis [59]. However, recent advancements in the preparative procedures of tpm ligands have provided easy access to this class of ligand [59]. The molecular structure of tpm is illustrated in Figure 13.
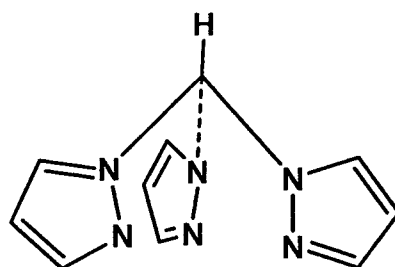
Figure 13. Tris(pyrazolyl)methane.

Intrigued and inspired by the work of Dyson and Sadler, the intent of this research project was to synthesize a variety of ruthenium(II) pseudo piano stool complexes containing tpm along with a variety of auxiliary ligands, and screen them for their *in vitro* antiproliferative properties using the MTT assay. The molecular designs were based on the assumption that DNA would be the cellular target of these compounds. The auxiliary ligands that we wished to use in this

study were: ethylenediamine, 1,2-diaminobenzene, trimethylphosphite and a variety of monodentate and bidentate phosphines. The general molecular structure of the target compounds are depicted in Figure 14 along with the structure of the auxiliary ligands.

$[...]^+$ PF_6^-

Where L,L =

H_2N—NH_2

a

NH_2 / NH_2 (1,2-diaminobenzene)

b

$2\left(\text{trimethylphosphite} \right)$

c

$2\left(Ph_2\!-\!\overset{P}{\underset{Me}{|}}\!-\!Ph_2 \right)$

d

$Ph_2P(CH)_nPPh_2$

n= 1 (e)
   2 (f)
   3 (g)
   4 (h)

Figure 14. General structure of the ruthenium(II) target compounds. Molecular structure of the chelating ligands are also provided: (a) en, (b) dab, (i) trimethylphosphite,

(h) methyldiphenylphosphine,(d) bis(diphosphino)methane (dppm),

(e) 1,2bis(diphenylphosphino)ethane (dppe), (f) 1,3- bis(diphenylphosphino)propane (dppp),

(g) 1,4-bis(diphenylphosphino)butane (dppb).

The rationale stimulating the use of tpm was one of derivatizability. It is apparent from the study of the aforementioned metal-based anticancer compounds that ligand variation can be used to modify the activity of these compounds and "fine tune" their antiproliferative effects. With this in mind, we chose to incorporate tpm in our molecular design because tpm is easily modified at positions on the pyrazole rings and at the central carbon atom. It was hoped that the tpm ligand would confer aqueous solubility on the target complexes as has been shown for these types of ligands in other systems [59,60]. Furthermore, it was anticipa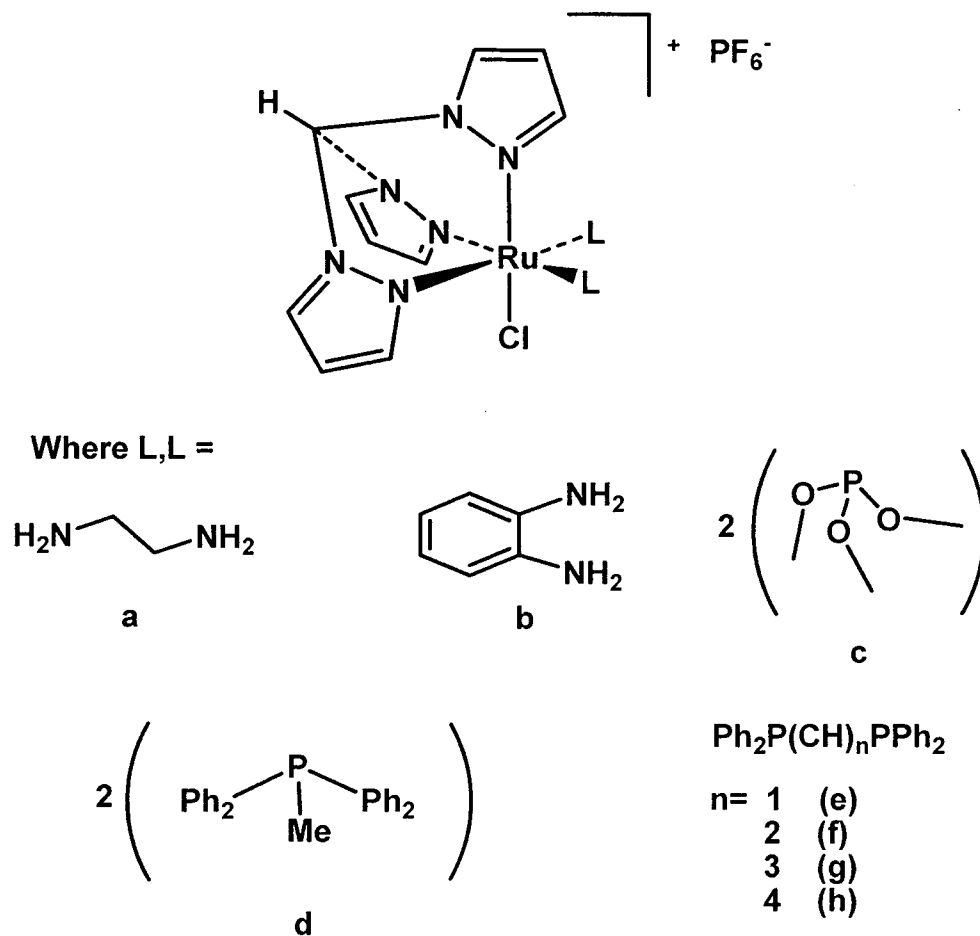ted that the rings of tpm might intercalate with DNA and increase the antiproliferative effects of these complexes. However, if these properties were absent from the target compounds simple functionalization of the tpm ligand could be used to modify these parameters.

As for the auxiliary ligands, the chloride ligand is a good leaving group, and the exchange of this ligand for an aqua ligand may serve as a mechanism of activation of these compounds toward biomolecular targets. The ethylenediamine and 1,2-diaminobenze were chosen because the complexes incorporating these ligands in the Sadler-type model have shown excellent anticancer activity [48].

The motivation for the phosphite ligand was the possibility of the oxygen atoms to be involved in hydrogen bonding interactions with the amino hydrogens of adenine. The bidentate phosphines were included in the target compounds due to the fact that excellent antiproliferative activity has been achieved with [Au(dppe)$_2$]Cl and its derivatives [17,18,20]. The possibility of the phenyl rings intercalating into the DNA framework was also a motive to utilize these ligands.

Furthermore, slight variation of the aliphatic backbone of the phosphine ligands would provide insight as to whether the size of this feature has any influence on the cytotoxicity of these complexes.

The cell lines that were used in this study were the HeLa and MCF-7 cell lines. These cells were derived from cervical and breast cancers, respectively. The reasoning behind their use in this project, besides the fact that they were readily available, was because Hela and MCF-7 cells represent tumour lines from common cancer sites. Furthermore, they are extensively studied cell lines that are commonly used for cytotoxicity testing.

3. Experimental

3.1 General Considerations

Unless otherwise stated, all experiments and manipulations were conducted under an inert atmosphere of prepurified N_2 using standard Schlenk techniques. Distilled, deionized water was stored in a bulb with a Teflon tap, and purged with N_2 prior to use. Methanol, acetonitrile and DMSO were dried and stored over activated 4A molecular sieves in bulbs with Teflon taps, and purged with N_2 before use. All other bulk solvents used in large-scale preparations were pre-dried over activated 4A molecular sieves, passed through a column of alumina, purged with N_2 and stored over 4A molecular sieves in bulbs with Teflon taps [61]. Deuterated solvents were used as received and stored in a bulb with a Teflon tap. NMR spectra (^{1}H and ^{31}P{^{1}H}) were obtained using a Varian Unity INOVA 500 MHz spectrometer, with chemical shifts (in ppm) referenced to residual protio solvent peaks (^{1}H) or external 85% H_3PO_4 (^{31}P). Elemental analyses were performed on a CEC 240XA analyzer by the Lakehead University Instrumentation Laboratory. The ruthenium precursor (κ^3-tpm)$RuCl_3 \cdot 1.5H_2O$ [62] and [(η^6-p-cymene)RuCl(κ^2-dppp)]Cl [63] were prepared according to the literature procedures.

3.2 Synthesis of [(κ³-tpm)RuCl(MeCN)₂][PF₆], 1

The complex $(tpm)RuCl_3\cdot1.5H_2O$ (0.548 g, 1.22 mmol) and Zn dust (0.145 g, 2.22 mmol) were suspended in MeCN (30 mL). The solution was allowed to stir at reflux for 2 hr. The mixture was then filtered through Celite yielding a clear yellow-brown filtrate. The volatiles were removed under reduced pressure and the residue was redissolved in methanol (10 mL). NH_4PF_6 (0.200 g, 1.23 mmol) was added and the mixture was allowed to stir at room temperature for 11 hr. The mixture was passed through a frit yielding a grey-green solid. The solid was washed with 10 mL each of H_2O and acetone, followed by 30 mL of diethyl ether. After drying under reduced pressure, a grey solid was obtained. Yield: 59%. Anal. calcd. for $C_{14}H_{16}ClF_6N_8PRu\cdot H_2O$: C, 28.22; H, 3.04; N, 18.81. Found: C, 28.06; H, 2.88; N, 18.44. Proton NMR spectroscopy provided evidence for the inclusion of H_2O in the sample. ^1H NMR (499.9 MHz, D_2O, 22°C): 9.22 (s, 1H, Pz_3CH), 8.16 (m, 2H, Pz), 8.13 (m, 1H, Pz), 7.87 (m, 3H, Pz), 6.42 (m, 2H,Pz), 6.38 (m, 1H, Pz), 2.37 (s, 6H, MeCN).

3.3 Synthesis of [(κ³-tpm)RuCl(DMSO)₂][PF₆], 2

The complex $(tpm)RuCl_3\cdot1.5H_2O$ (0.215 g, 0.479 mmol) and Zn dust (0.050 g, 0.765 mmol) were suspended in MeOH (30 mL). Next, DMSO (333 µL, 4.69 mmol) was added. The solution was allowed to stir at reflux for 21 hr. After this time, the residual Zn had deposited on the walls of the flask leaving a clear

yellow supernatant. Once cooled, the mixture was then filtered through Celite

yielding a clear yellow filtrate. The volatiles were removed under reduced

pressure and the residue was redissolved in methanol (10 mL). NH_4PF_6 (0.078 g,

0.479 mmol) was added and a yellow solid precipitated immediately. The solid

was filtered off, and washed with 10 mL each of MeOH, acetone and diethyl

ether. The product was dried under reduced pressure. Yield: 63%. Anal. calcd.

for $C_{14}H_{22}ClF_6N_6O_2PRuS_2$: C, 25.79; H, 3.40; N, 12.89. Found: C, 26.05; H, 3.57;

N, 13.09. ^1H NMR (499.9 MHz, D_2O, 22°C): 9.54 (s, 1H, Pz_3CH), 8.39 (m, 1H,

Pz), 8.28 (m, 2H, Pz), 8.12 (m, 1H, Pz), 8.04 (m, 2H, Pz), 6.59 (m, 1H, Pz), 6.50

(m, 2H, Pz), 3.32 (s, 6H, DMSO), 2.96 (s, 6H, DMSO).

3.4 Synthesis of [(κ^3-tpm)RuCl(P(OMe)$_3$)$_2$][PF$_6$], 3

A flask was charged with [(κ^3-tpm)RuCl$_3$]·1.5H$_2$O (0.134 g, 0.299 mmol)

and Zn dust (0.030 g, 0.459 mmol). The contents were suspended in MeOH (10

mL). The phosphite P(OMe)$_3$ (78 μL, 0.661 mmol) was added and the mixture

was allowed to stir at reflux for 4 hr. The resulting solution, which consisted of a

clear yellow supernatant with residual Zn, was filtered through Celite into a flask

containing NH_4PF_6 (0.086 g, 0.528 mmol). The mixture was stirred at room

temperature for 30 mins before the volatiles were removed under reduced

pressure. The yellow solid was triturated in diethyl ether (20 mL) and

recrystallized by slow diffusion using MeOH and diethyl ether. Excess NH_4PF_6

was removed by washing the grey-yellow solid with a small amount of H_2O. Yield:

36 %. Anal. calcd. for $C_{16}H_{28}ClF_6N_6O_6P_3Ru \cdot 1/3H_2O$: C, 25.64; H, 3.84; N, 11.22.

Found: C, 25.11; H, 3.87; N, 10.87. Proton NMR spectroscopy provided evidence

for the inclusion of H_2O in the sample. ^1H NMR (499.9 MHz, $CDCl_3$, 22°C) 9.19

(s, 1H, Pz$_3$CH), 8.42 (m, 1H, Pz), 8.32 (m, 2H, Pz), 1.17 (m, 2H, Pz), 7.93 (m,

1H, Pz), 6.47 (m, 2H, Pz), 6.39 (m, 1H, Pz), 3.60 (br m, 18H, POCH$_3$). $^{31}P\{^1H\}$

NMR (202.3 MHz, $CDCl_3$, 22°C): 139.3 (s, P(OMe)$_3$), -143.6

(septet, PF$_6^-$).

3.5 Synthesis of [(κ^3-tpm)RuCl(PMePh$_2$)$_2$][PF$_6$], 4

The complex [(κ^3-tpm)RuCl$_3$]·1.5H$_2$O (0.180 g, 0.401 mmol) and Zn dust

(0.073 g, 1.12 mmol) were added to a flask, and suspended in MeOH (20 mL).

The phosphine PMePh$_2$ (165 μL, 0.889 mmol) was added via syringe and the

mixture was allowed to stir at reflux for 8 hr. The flask was allowed to cool to

room temperature before filtering the contents through Celite, yielding a clear

orange/yellow filtrate. The volume of the filtrate was reduced to ~10 mL under

reduced pressure, and then NH$_4$PF$_6$ (0.065 g, 0.399 mmol) was added. The

mixture was stirred at room temperature for 8 hr and then left in an ice bath

overnight. The mixture was then filtered, and diethyl ether (10 mL) was added to

the filtrate precipitating a white solid. The solution was filtered to remove the

solid, and then the volatiles were removed from the orange-yellow filtrate under

reduced pressure yielding an orange-yellow solid. The product was stirred in H$_2$O

(30 mL), washed with diethyl ether (20 mL) and finally dried under reduced

pressure. Yield: 32 %. Anal. calcd. for $C_{36}H_{36}ClF_6N_6P_3Ru$: C, 48.25; H, 4.05; N, 9.38. Found: C, 48.16; H, 3.98; N, 9.06. ^{1}H NMR (499.9 MHz, $CDCl_3$, 22°C): 9.49 (s, 1H, Pz_3CH), 8.92 (br m, 1H, Pz), 8.41 (br m, 2H, Pz), 7.40-7.16 (overlapping m, 16H, Ph), 7.07 (br m, 1H, Pz), 6.92 (m, 4H, Ph), 5.85 (br m, 2H, Pz), 6.30 (m, 1H, Pz), 5.92 (m, 2H, Pz), 1.94 (m, 6H, PMePh$_2$). ^{31}P{^{1}H} NMR (202.3 MHz, $CDCl_3$, 22°C): 25.9 (s, PMePh$_2$), -142.6 (septet, PF$_6^-$).

3.6 Synthesis of [(κ^3-tpm)RuCl(κ^2-dppm)][PF$_6$], 5

The complex [(κ^3-tpm)RuCl$_3$]•1.5 H_2O (0.326 g, 0.848 mmol), dppm (0.326 g, 0.848 mmol), and Zn dust (0.050 g, 0.765 mmol) were placed in a flask and suspended in MeOH (30 mL). The solution was stirred at reflux for 12 hr. The flask was allowed to cool to room temperature before filtering the contents through Celite into a flask containing NH$_4$PF$_6$ (0.093 g, 0.570 mmol). Immediately, a bright yellow precipitate formed in the filtrate and the residual product was transferred using MeOH (10 mL). The filtrate was stirred at 80°C for 1 hr. The mixture was cooled to room temperature before filtration, isolating the light yellow solid. The solid was washed with MeOH (10 mL) and diethyl ether (10 mL). Yield: 63 %. Anal. calcd. for $C_{35}H_{32}ClF_6N_6P_3Ru$•$H_2O$: C, 46.81; H, 3.82; N, 9.35. Found: C, 46.59; H, 3.69; N, 9.12. Proton NMR spectroscopy provided evidence for the inclusion of H_2O in the sample. ^{1}H NMR (499.9 MHz, DMSO, 22°C): 9.93 (s, 1H, Pz_3CH), 8.55 (br m, 2H, Pz), 8.39 (br m, 1H, Pz), 7.75- 7.72 (overlapping m, 2H Pz, 4H Ph), 7.46 (m, 4H, Ph), 7.35 (m, 2H, Ph), 7.21 (br m, 8

H, Ph), 6.69 (br m, 2H, Pz), 5.88 (m, 1H, Pz), 5.77 (m, 1H, $Ph_2CH_aH_bPPh_2$), 5.57 (m, 1H, Pz), 5.07 (m, 1H, $Ph_2CH_aH_bPPh_2$). $^{31}P\{^1H\}$ NMR (202.3 MHz, DMSO, 22°C): 8.31 (s, dppm), -144.2 (septet, PF_6^-).

3.7 Synthesis of [(κ^3-tpm)RuCl(κ^2-dppe)][PF$_6$], 6

3.7.1 Method (a): Zn Reduction

A flask was charged with [(κ^3-tpm)RuCl$_3$]•1.5 H$_2$O (0.194 g, 0.432 mmol), dppe (0.258 g, 0.648 mmol) and Zn dust (0.062 g, 0.948 mmol). Next, MeOH (20 mL) was added and the solution was allowed to stir at reflux for 5 hours. The flask was allowed to cool to room temperature before filtering the contents through Celite into a separate flask containing NH_4PF_6 (0.070 g, 0.429 mmol). The mixture was stirred at reflux for 1 hr before the volatiles were removed under reduced pressure. The orange/brown residue was redissolved in CH_2Cl_2 (10 mL) and filtered through Celite. The volatiles were removed from the filtrate under reduced pressure yielding an orange-yellow solid. The solid was washed with H$_2$O (30 mL) followed by diethyl ether (20 mL). The product was dried under reduced pressure. Yield: 61%. Anal. calcd. for $C_{36}H_{34}ClF_6N_6P_3Ru$: C, 48.36; H, 3.83; N, 9.40. Found: C, 48.29; H, 3.92; N, 8.52. The ^1H and $^{31}P\{^1H\}$ NMR spectra of **6** were identical to those reported in the literature [64].

3.7.2 Method (b): Ligand Substitution of 2

Complex **2** (0.039 g, 0.060 mmol) and dppe were placed in a flask and suspended in chlorobenzene (10 mL). The solution was allowed to stir at reflux for 19 hr. The clear yellow solution was allowed to cool to room temperature and the volatiles were removed under reduced pressure. The yellow residue was washed with diethyl ether (10 mL). The ^{1}H and ^{31}P{^{1}H} NMR spectra of **6** were identical to those reported in the literature [64].

3.8 Synthesis of [(κ^3-tpm)RuCl(κ^2-dppp)][PF$_6$], 7

A flask was charged with (tpm)RuCl$_3$·1.5H$_2$O (0.243 g, 0.541 mmol), dppp (0.224 g, 0.543 mmol) and Zn dust (0.055 g, 0.841 mmol). Next, MeOH (30 mL) was added and the solution was allowed to stir at reflux for 25 hours. After this time, a dark green solid had deposited from a clear orange supernatant. The mixture was allowed to cool to room temperature before filtering through Celite into a flask containing NH$_4$PF$_6$ (0.088 g, 0.540 mmol). The mixture was stirred at reflux for 1 hr before the volatiles were removed under reduced pressure. The green-yellow residue was redissolved in CH$_2$Cl$_2$ (20 mL) and filtered through Celite. The volatiles were removed from the orange-yellow filtrate under reduced pressure yielding an orange-yellow solid. The solid was washed with H$_2$O (30 mL) followed by diethyl ether (20 mL). The solid was dried under reduced pressure. Yield: 47%. Anal. calcd. for C$_{37}$H$_{36}$ClF$_6$N$_6$P$_3$Ru·H$_2$O: C, 47.98; H, 4.13; N, 9.08. Found: C, 48.03; H, 3.97; N, 8.93. Proton NMR spectroscopy provided

evidence for the inclusion of H_2O in the sample. ^1H NMR (499.9 MHz, $CDCl_3$, 22°C): 9.11 (s, 1H, Pz_3CH), 8.30 (br m, 2H, Pz), 8.20 (br m, 1H, Pz), 7.74 (br m, 4H, Ph), 7.43 (m, 2H, Ph), 7.34 (m, 4H, Ph), 7.31 (m, 2H, Ph), 7.10 (m, 4H, Ph), 6.65 (br m, 2H, Pz), 6.56 (br m, 4H, Ph), 6.12 (m, 2H, Pz), 5.32 (m, 2H, Pz), 5.08 (m, 1H, Pz), 3.01 (m, 2H, $Ph_2PCH_2CH_2CH_2PPh_2$), 2.93 (m, 1H, $Ph_2PCH_2CH_aH_bCH_2PPh_2$), 2.88 (m, 2H, $Ph_2PCH_2CH_2CH_2PPh_2$), 2.38 (m, 1H, $Ph_2PCH_2CH_aH_bCH_2PPh_2$). $^{31}P\{^1H\}$ NMR (202.3 MHz, $CDCl_3$, 22°C): 32.9 (s, dppp), -142.6 (septet, PF_6^-).

3.9 X-ray Crystallographic Study of Complex 7

Crystal Data Collection

A crystal of complex **7** (yellow, block-shaped, size 0.25 × 0.10 × 0.08 mm) was mounted on a glass fibre with grease and cooled to -93 °C in a stream of nitrogen gas controlled with a Cryostream Controller 700. Data collection was performed on a Bruker SMART APEX II X-ray diffractometer with graphite-monochromated Mo K_α radiation (λ = 0.71073 Å), operating at 50 kV and 30 mA over 2θ ranges of 4.14 ~ 52.00°. No significant decay was observed during the data collection.

Crystal Structure Solution and Refinement

Data were processed on a PC using the Bruker AXS Crystal Structure Analysis Package [65]: data collection: APEX2; cell refinement: SAINT; data reduction: SAINT; structure solution: XPREP and SHELXTL; and structure refinement: SHELXTL. Neutral atom scattering factors were taken from Cromer and Waber [66]. The crystal is monoclinic space group $P2_1/c$, based on the systematic absences, E statistics and successful refinement of the structure. Unit cell data: $a = 9.5060(2)$ Å, $b = 15.2172(3)$ Å, $c = 25.8550(5)$ Å, $\alpha = 90°$, $\beta = 95.2260(10)°$, $\gamma = 90°$, $Z = 4$, $V = 3724.50(13)\square^3$, D(calc) = 1.620 g/cm^3. The structure was solved by direct methods. Full-matrix least-square refinements minimizing the function $\sum w(F_{o2} - F_{c2})^2$ were applied to the compound. All non-hydrogen atoms were refined anisotropically. All of the other H atoms were placed in geometrically calculated positions, with C-H = 0.95 (aromatic) and 0.99 Å (CH$_2$), and refined as riding atoms, with Uiso(H) =1.2 Ueq(other C). The PF$_6^-$ anion is disordered, and the SHELX command PART and EADP were used to resolve the disorder. Convergence to final $R_1 = 0.0398$ and $wR_2 = 0.0948$ for 5892 ($I>2\sigma(I)$) independent reflections, and $R_1 = 0.0531$ and $wR_2 = 0.1047$ for all 7299 (R(int) = 0.0305) independent reflections, with 479 parameters and 0 restraints, were achieved [67]. The largest residual peak and hole to be 1.082 and -0.853 $e/$Å^3, respectively. Graphical representation of the structure was produced using ORTEP-3 [68].

Table 1. Crystal data and structure refinement for **7**.

Empirical formula	$C_{37}H_{36}ClF_6N_6P_3Ru$
Formula weight	908.15
Temperature	180(2) K
Wavelength	0.71073 Å
Crystal system	Monoclinic
Space group	P2(1)/c
Unit cell dimensions	a = 9.5060(2) Å $\qquad \alpha$= 90°.
	b = 15.2172(3) Å $\qquad \beta$= 95.2260(10)°.
	c = 25.8550(5) Å $\qquad \gamma$ = 90°.
Volume	3724.50(13) Å^3
Z	4
Density (calculated)	1.620 Mg/m^3
Absorption coefficient	0.690 mm^{-1}
F(000)	1840
Crystal size	0.25 x 0.10 x 0.08 mm^3
Theta range for data collection	2.07 to 26.00°.
Index ranges	-11<=h<=9, -18<=k<=10, -26<=l<=31
Reflections collected	16901
Independent reflections	7299 [R(int) = 0.0305]
Completeness to theta = 26.00°	99.8 %
Absorption correction	Multi-scan
Max. and min. transmission	0.9469 and 0.8465
Refinement method	Full-matrix least-squares on F^2
Data / restraints / parameters	7299 / 0 / 479
Goodness-of-fit on F^2	1.022
Final R indices [I>2sigma(I)]	R1 = 0.0398, wR2 = 0.0948
R indices (all data)	R1 = 0.0531, wR2 = 0.1047
Largest diff. peak and hole	1.082 and –0.853 e.Å^{-3}

3.10 Synthesis of [(κ³-tpm)RuCl(κ²-dppb)][PF₆], 8

A flask was charged with (tpm)RuCl₃·1.5H₂O (0.100 g, 0.223 mmol), dppb (0.105 g, 0.246 mmol) and Zn dust (0.032 g, 0.490 mmol). Next, MeOH (10 mL) was added and the solution was allowed to stir at reflux for 6 hours. After this time, a dark green solid had deposited from a clear bright orange supernatant. The flask was allowed to cool to room temperature before filtering the contents through Celite into a flask containing NH_4PF_6 (0.036 g, 0.221 mmol). The mixture was stirred at room temperature for 19 hours. During this time, a bright yellow solid deposited. The solid was isolated by filtration, and washed with H_2O (30 mL) followed by diethyl ether (20 mL). The solid was dried under reduced pressure. Yield: 19%. Anal. calcd. for $C_{38}H_{38}ClF_6N_6P_3Ru \cdot H_2O$: C, 46.81; H, 3.82; N, 9.35. Found: C, 46.59; H, 3.69; N, 9.12. Proton NMR spectroscopy provided evidence for the inclusion of H_2O in the sample. ^1H NMR (499.9 MHz, CDCl₃, 22°C): 9.10 (s, 1H, Pz₃CH), 8.26 (br, 2H, Pz), 8.23 (br, 1H, Pz), 7.56 (br m, 4H, Ph), 7.41 (br m, 2H, Ph), 7.30-7.26 (br m, 6H, Ph), 7.06 (br m, 4H, Ph), 6.72 (br m, 2H, Pz), 6.61 (br m, 4H, Ph), 6.08 (br, 2H, Pz), 6.02 (br m, 1H, Pz), 5.50 (br m, 1H, Pz), 3.00 (br, CH_2 of dppb), 2.78 (br, CH_2 of dppb), 2.62 (br, CH_2 of dppb), 2.13 (br, CH_2 of dppb). $^{31}P\{^1H\}$ NMR (202.3 MHz, CDCl₃, 22°C): 36.3 (s, dppb), -142.6 (septet, PF₆⁻).

3.11 Attempted Synthesis of [(κ³-tpm)RuCl(en)][X], 9 (X=Cl⁻, PF₆⁻)

3.11.1 Method (a): Zn Reduction

A flask was charged with [(κ³-tpm)RuCl₃]·1.5H₂O (0.211 g, 0.470 mmol) and Zn dust (0.046 g, 0.704 mmol). MeOH was added (30 mL) followed by en (333 μL, 4.97 mmol) and the mixture was stirred at reflux for 16 hr. The resulting orange-red solution was filtered through Celite and the volatiles were removed from the filtrate yielding a red solid. The solid was washed with diethyl ether (10 mL). The ¹H NMR spectrum was inconclusive and showed that a variety of complexes were present.

3.11.2 Method (b): Reduction using Triethylamine

[(κ³-tpm)RuCl₃]·1.5H₂O (0.527 g, 1.17 mmol) was placed in a flask and suspended in toluene (20 mL). The ligand en (2.0 mL, 30 mmol) was added to the flask drop-wise followed by triethylamine (NEt₃) (4.0 mL, 29 mmol). The solution was allowed to stir at reflux for 22 hr. By the end of the reflux, the mixture consisted of a clear supernatant with a dark burgundy residue on the bottom of the flask. The supernatant was decanted and the residue was dissolved in EtOH (10 mL). The product was precipitated from solution by the addition of diethyl ether (30 mL). This purification procedure was repeated four times before the product was isolated via filtration. The residual product was transferred to a frit using 20 mL of diethyl ether and the brown solid was dried under reduced pressure. Crude yield: 86 %. Purification was performed by

dissolving the product in H_2O and filtering the solution through silica (1 cm length, 3 cm diameter). The volatiles were removed from the eluent by evaporation yielding a light brown solid. ^1H NMR (499.9 MHz, D_2O, 22°C): 9.12 (s, 1H, Pz_3CH), 8.19 (m, 2H, Pz), 8.14 (m, 1H, Pz), 7.96 (m, 2H, Pz), 7.68 (m, 1H, Pz), 6.43 (m, 2H, Pz), 6.33 (m, 2H, Pz) 4.22 (br m, 2H, en), 4.10 (br m, 2H, en), 3.90 (br m, 2H, en), 2.83 (br m, 2H, en), 2.74 (br m, 2H, en), 2.37 (br m, 2H, en).

3.11.3 Method (c): Ligand Substitiution of 1

Complex 1 (0.105 g, 0.182 mmol) was placed in a flask and suspended in chlorobenzene (10 mL). The ligand en was added and the mixture was allowed to stir at 140 °C for 3 hr. The clear brown-red supernatant was removed and the red solid material was washed with diethyl ether (20 mL) and acetone (20 mL). The remaining volatiles were removed under reduced pressure yielding a red-pink solid. ^1H NMR (499.9 MHz, DMSO, 22°C) 10.15 (s, 1H, Pz_3CH), 8.52- 8.49 (overlapping br m, 5 H, Pz), 7.89 (d, 1 H, Pz, J= 1.5), 6.63- 5.57 (overlapping br m, 3 H, Pz), 5.34 (br m, 2 H), 4.76 (br m, 2 H), 4.39 (br m, 2 H), 2.72- 2.67 (overlapping br m, 4 H) 1.92 (br m, 2 H).

3.11.4 Method (d): Ligand Substitution of 2

In a typical procedure, complex 2 was placed in a flask and dissolved/suspended in a solvent. The ligand en was added and the mixture was allowed to stir at reflux. The volatiles were removed and the solid was washed with diethyl ether. The ^1H spectra obtained were identical to the spectrum

obtained for **2** except that the signal pertaining to the apical H of the tpm ligand was absent.

3.12 Attempted Synthesis of [(κ³-tpm)RuCl(dab)][X], 10 (X=Cl⁻,PF6⁻)

3.12.1 Method (a) Zn Reduction

In a typical process, [(κ³-tpm)RuCl₃]·1.5H₂O and dab were placed in a flask and suspended in a solvent. The mixture was allowed to stir at reflux and during this time the solution or suspended material turned dark burgundy. The volatiles were removed and the product was washed with diethyl ether or acetone. ¹H NMR spectra were inconclusive and revealed many signals.

3.12.2 Method (b) Reduction using NEt₃

A flask was charged with the complex [(κ³-tpm)RuCl₃]·1.5H₂O (0.0984 g, 0.219 mmol) and dab (0.060 g, 5.48 mmol). Toluene was added (10 mL) was added followed by NEt₃ (764 μL, 5.48 mmol) and the mixture was stirred at reflux for 20 hr. The volatiles were removed from the dark purple solution under reduced pressure yielding a residue of similar colour. The product was washed with diethyl ether (2 x 10 mL). The ¹H NMR spectrum was inconclusive and showed the formation of a multitude of compounds.

3.12.3 Method (c): Ligand Substitiution of 1

In a typical procedure, complex **1** and dab were placed in a flask and suspended in a solvent. The mixture was allowed to stir at room temperature or reflux. The volatiles were removed form the mixture and the product was washed with diethyl ether and/or acetone. In all reactions a deep red-burgundy residue was obtained. ^{1}H NMR spectra obtained were inconclusive as to the formation of the desired product and often consisted of many signals.

3.12.4 Method (d): Ligand Substitution of 2

A flask was charged with complex **2** (0.134 g, 0.206 mmol) and dab (0.025 g, 0.227 mmol). The contents were suspended in nitromethane and stirred at reflux for 2 hr. The dark red-burgundy solution was filtered and the filtrate was placed in an evaporating dish and placed in the fume hood. When evaporation was complete, the dark red residue was redisolved in MeOH (10 mL) and transferred to a flask. The volatiles were removed and the residue was washed twice with diethyl ether. The ^{1}H NMR was inconclusive and contained at least 3 tpm containing compounds due to the presence of 3 separate apical H peaks.

3.13 Growth Inhibition Assays

3.13.1 Cell culture conditions and cell proliferation assays.

The MCF-7 and HeLa cancer cell lines were grown in Dulbecco's Modified Eagle's Medium (Sigma) containing 10% fetal bovine serum (PAA Laboratories) at 37 °C in a 5% CO_2 humidified atmosphere. Measurement of cell proliferation was determined using the 3-(4,5-dimethylthiazol-2-yl)-2,5-diphenyltetrazolium bromide (MTT) assay [69]. Briefly, 2000 cells were plated out into each well of a 96-well plate and allowed to adhere overnight. The ruthenium compounds (which were dissolved in DMSO, and diluted with tissue culture medium) were added at increasing concentrations (0–50 μM, 8 wells per concentration). The cells were incubated in the presence of each ruthenium compound for 72 hours. MTT reagent (Sigma), dissolved in phosphate buffered saline, was added to each well to a final concentration of 0.5 mg/mL, and the cells were incubated for four additional hours. Following this time, the medium containing the MTT reagent was aspirated off and replaced with 100 μL DMSO. The purple-coloured formazan product in each well was measured by absorbance in a microplate reader (PowerWave XS, Bio-Tek) at a wavelength of 490 nm. The IC_{50} value for each compound tested was determined by plotting concentration vs. percent absorbance obtained in the MTT assay. Cisplatin was used as prepared for injection in aqueous (saline) solution (i.e. cisplatin was not dissolved in DMSO for the MTT assays).

3.13.2 MTT Assay Results

The antiproliferative effects of complexes **1-8**, $[(\eta^6\text{-}p\text{-cymene})RuCl(\kappa^2\text{-}dppp)]Cl$, cisplatin and doxorubacin were determined using the MTT assay. Growth inhibition curves can be found in Appendix A.

4. Results and Discussion

4.1 Introduction

The primary obstacle that was encountered at the onset of this project was the lack of convenient starting materials for tpm-ruthenium(II) complexes. Although there are a few compounds that have been reported in the literature that, upon first glance, appear as though they may serve as useful precursors to the target molecules of this project, details regarding the synthesis of these compounds, conditions that are required for subsequent ligand substitution reactions or available methods to reduce ruthenium(III) materials to the desired ruthenium(II) species limit the use of these compounds as opportune starting materials. For example, the complex $[(\kappa^3\text{-tpm})RuCl(COD)][PF_6]$ (COD = 1,5 cylooctadiene) has been reported in the literature and has been used to prepare complex **4** (*vide infra*), however the preparation was undesirable, requiring harsh conditions (reflux in dimethylformamide for a number of hours) and column chromatography only to obtain a meager yield [64].

A great deal of time and effort was expended in performing scouting reactions with various prospective starting materials in order to develop a versatile and convenient synthetic route to the target compounds. Although not all of our target compounds were synthesized in the timeframe of this project, a versatile and convenient route was discovered which allowed the synthesis of a number of our target molecules and two potentially useful precursors for the

synthesis of various other tpm-ruthenium(II) compounds. Furthermore, the preliminary results regarding the anticancer properties of the complexes synthesized in this project are very promising, and suggest further study to uncover the biological activity of these novel compounds.

4.2 Synthesis and Characterization of Solvento Complexes 1 and 2

A common method of synthesizing desired coordination compounds from simple starting complexes involves trapping them as solvento complexes. The lack of success with the more common starting materials served as inspiration to synthesize tpm-ruthenium solvento compounds with the prospect of substituting the solvent ligands with the desired ligands of our target compounds. It was this direction that would eventually lead to the versatile synthetic procedure that we were seeking.

An interesting study reporting the synthesis of tpm-ruthenium(II) compounds from the readily available starting material (κ^3-tpm)RuCl$_3$, using elemental zinc as a reducing agent, was reported in the literature; however, preparative details were not described, except that the reactions were performed in either ethanolic or aqueous media [70].

In light of this study, we decided to experiment with zinc reduction reactions involving (κ^3-tpm)RuCl$_3\cdot$1.5H$_2$O and coordinating solvents. It was found that refluxing (κ^3-tpm)RuCl$_3\cdot$1.5H$_2$O and zinc dust in acetonitrile followed by a salt metathesis reaction with NH$_4$PF$_6$ provided the solvento complex 1 as a grey

solid. Furthermore, a similar reaction, but replacing acetonitrile with a methanolic

solution of DMSO, afforded the solvento complex **2** as a bright yellow solid.

The NMR spectra of these compounds reflect the C_s symmetry of the

molecules in that there are six different pyrazole signals integrating 2:1:2:1:2:1

(Figure 15). This pattern arises due to the fact that the plane of symmetry of the
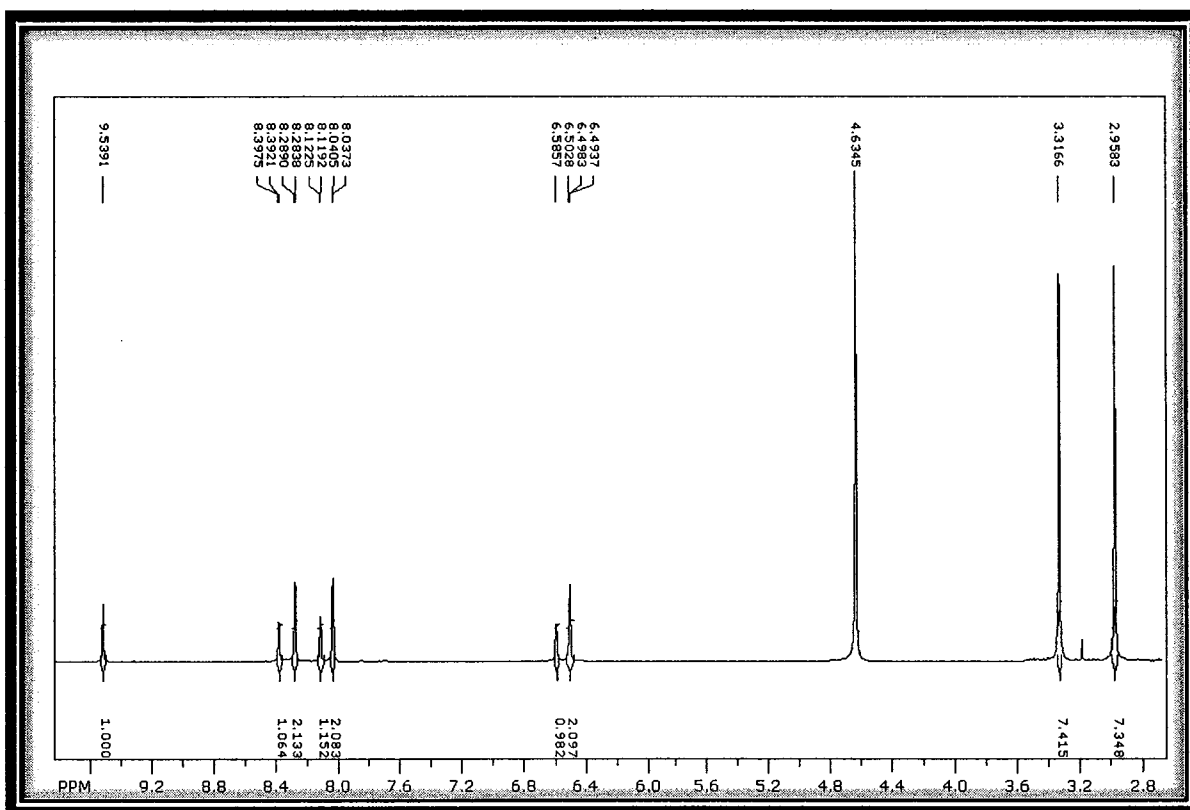

Figure 15. Proton NMR spectrum of complex **2**.

molecule passes through the chloride ligand and one of the tpm pyrazole rings

making two of the rings equivalent and one ring not equivalent, as illustrated in

Figure 16. Furthermore, a singlet pertaining to the proton on the bridgehead

carbon is present. These signals are characteristic of C_s symmetric tpm

compounds; a number of examples have been reported in the literature [64,70].
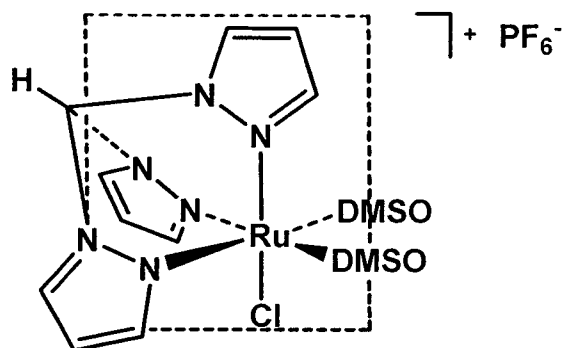
Figure 16. Molecular structure of **2** showing the chemical equivalence of two pyrazole rings due to the C_s symmetry of the complex.
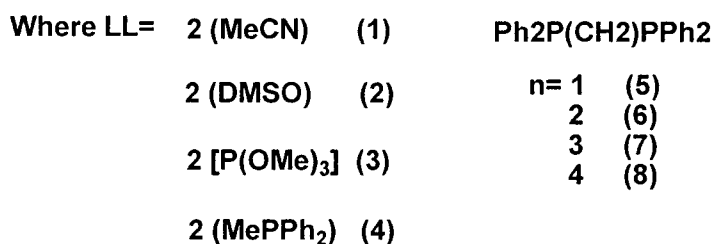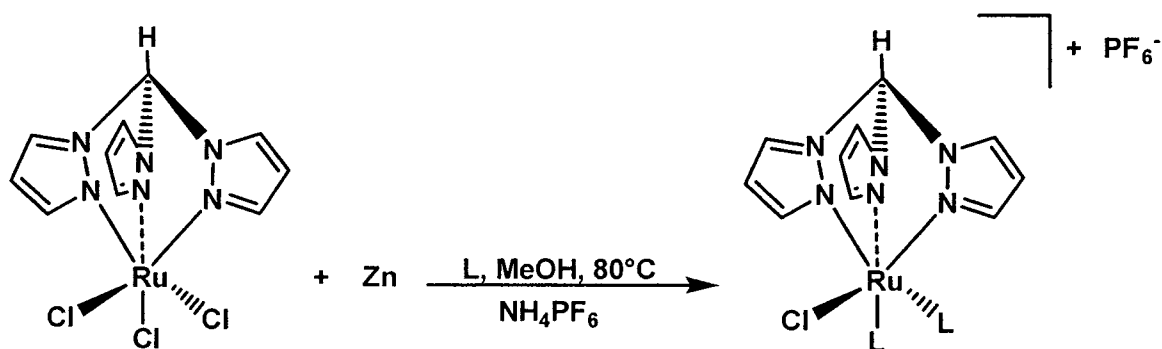
As for the solvento ligands, a singlet is observed for complex **1**, integrating

to six protons with respect to the bridgehead proton signal that pertains to the six

chemically equivalent protons of the two acetonitrile ligands [46,64,71]. The NMR

spectrum of complex **2** contains two singlets integrating to six protons each.

These peaks are attributed to the protons of the two inequivalent methyl groups

of the DMSO ligands (Figure 15) [72]. In each case, the solvento ligand signals

resonate upfield (3.4–2 ppm in D_2O) from those of the tpm ligand (9.5–6.3 ppm in

D_2O). For both complexes **1** and **2**, satisfactory elemental analyses were

obtained.

4.3 Synthesis and Characterization of Phosphine/Phosphite Complexes

4.3.1 Monodentate Phosphine/Phosphite Complexes: 3 and 4

Although the purpose of synthesizing the solvento complexes was to employ them as precursors to our target molecules, the success of the zinc reduction reactions prompted us to extend this reaction to include various phosphine/phosphite ligands as a direct route to our target compounds. It was found that this reaction could be modified to synthesize complexes 3-8 by simply refluxing a methanolic mixture of in the presence of zinc dust and the appropriate phosphine/phosphite ligand, followed by the addition of NH_4PF_6 as illustrated in Scheme 2.

The first compounds prepared by this route, complexes 3 and 4, are examples of monodentate bis-phosphine and bis-phosphite compounds. Both of these molecules display the same characteristic C_s symmetric tpm signature in the proton NMR spectrum as discussed for the solvento complexes 1 and 2. In addition, the proton NMR spectrum of complex 3 displayed a large singlet at 3.60 ppm ($CDCl_3$) integrating to eighteen protons with respect to the bridgehead proton signal of the tpm ligand. This large peak results from the eighteen equivalent methyl protons of the trimethylphosphite ligands. The phosphorus NMR spectrum exhibited a single peak at 139.3 ppm ($CDCl_3$) pertaining to the phosphite ligands suggesting they were equivalent. A septet was also present

Where LL= 2 (MeCN)   (1)   Ph2P(CH2)PPh2

2 (DMSO)   (2)   n= 1   (5)
                         2   (6)
2 [P(OMe)$_3$] (3)   3   (7)
                         4   (8)

2 (MePPh$_2$)   (4)

Scheme 2. Synthesis of compounds **1-8** using the versatile zinc reduction method.

upfield at -143.6 ppm in the phosphorus spectrum characteristic of the PF_6^-

counterion.

The proton NMR spectrum of complex **4** contained multiplets in the phenyl

region integrating to a total of twenty protons. These signals are attributed to the

phenyl protons of the methyldiphenylphosphine ligands. The methyl signal of

these ligands was present upfield at 1.94 ppm ($CDCl_3$) as a singlet integrating to

six protons with respect to the bridgehead tpm proton signal. The phosphorus

NMR spectrum of complex **4** revealed a singlet pertaining to the

methyldiphenylphosphine ligands and a septet arising from the PF_6^- counterion at

25.9 and -142.6 ppm ($CDCl_3$), respectively.

Both compounds **3** and **4** gave suitable elemental analyses. Complex **3** was partially hydrated as evidenced from the proton NMR spectrum, most likely resulting from the water wash in the preparation of this complex. This apparent hydration was taken into account when calculating the theoretical elemental composition, and afforded values that were agreeable with the experimental values obtained for this complex.

4.3.2 Bidentate Phosphine Complexes: 5-8

The success of the aforementioned zinc reduction reaction allowed us to focus our attention on bis(diphenylphosphino)alkane ligands, $Ph_2P(CH_2)_nPPh_2$ (n=1-4). These efforts led to the successful synthesis of the target compounds **5-8**.

As would be expected, the proton NMR spectra of compounds **5-8** were similar and revealed the characteristic C_s symmetric downfield tpm signals as discussed previously for complexes **1-4**. In addition, the proton spectra also contained phenyl signals arising from the phenyl groups on the bis(diphenylphosphino)alkane ligands with the correct integration of twenty protons. One differing aspect of the proton NMR spectra of these complexes was related to the signals produced by the protons located on the alkyl chain linking the phosphorus atoms of the chelating phosphine ligands. Thus, the proton NMR spectrum of complex **5**, $[(\kappa^3\text{-tpm})RuCl(\kappa^2\text{-dppm})]PF_6$, displayed two broad multiplets integrating to one proton each. The presence of these two signals indicates the chemical inequivalence of the protons situated on the methyl linker

between the two diphenylphosphine groups of the dppm ligand. Compound **6** displayed two broad multiplets, whereas compound **8** showed four broad multiplets, in their respective proton spectra that arose due to the plane of symmetry that bisects the dppe and dppb ligands of these compounds. Both the proton and phosphorus spectra obtained for complex **6** were identical to those previously reported in the literature for this complex [64]. The proton NMR spectrum of complex **7** revealed two sets of two multiplets with an integration ratio of 2:1 that also resulted from the plane of symmetry that bisects the dppp ligand (Figure 17).

One singlet was observed in each of the phosphorus NMR spectra of compounds **5-8** for the two equivalent phosphorus atoms located on the bidentate phosphine ligands. The phosphorus resonance frequencies of these complexes were similar to those of other ruthenium complexes containing the respective bis(diphenylphosphino)alkane ligands [63,64,73]. The presence of the PF_6^- was confirmed by the appearance of an upfield septet in the phosphorus NMR spectra pertaining to compounds **5-8**. It must be noted that, due to the ability of the dppb ligand to bridge metal centres [74], complex **8** may assume the alternative dimeric structure $\{[(\kappa^3- tpm)RuCl(\mu-dppb)]PF_6\}_2$. This alternative structure would provide NMR and microanalytical data parallel to that of the monomeric species. Unfortunately, an X-ray diffraction, mass spectrometry and molecular weight data for this compound were not obtained to verify this structural uncertainty. Elemental analysis data obtained for compounds **5-8** were in agreement with calculated theoretical values. In the instances where hydration

was evidenced by proton NMR, the calculation of theoretical values included the

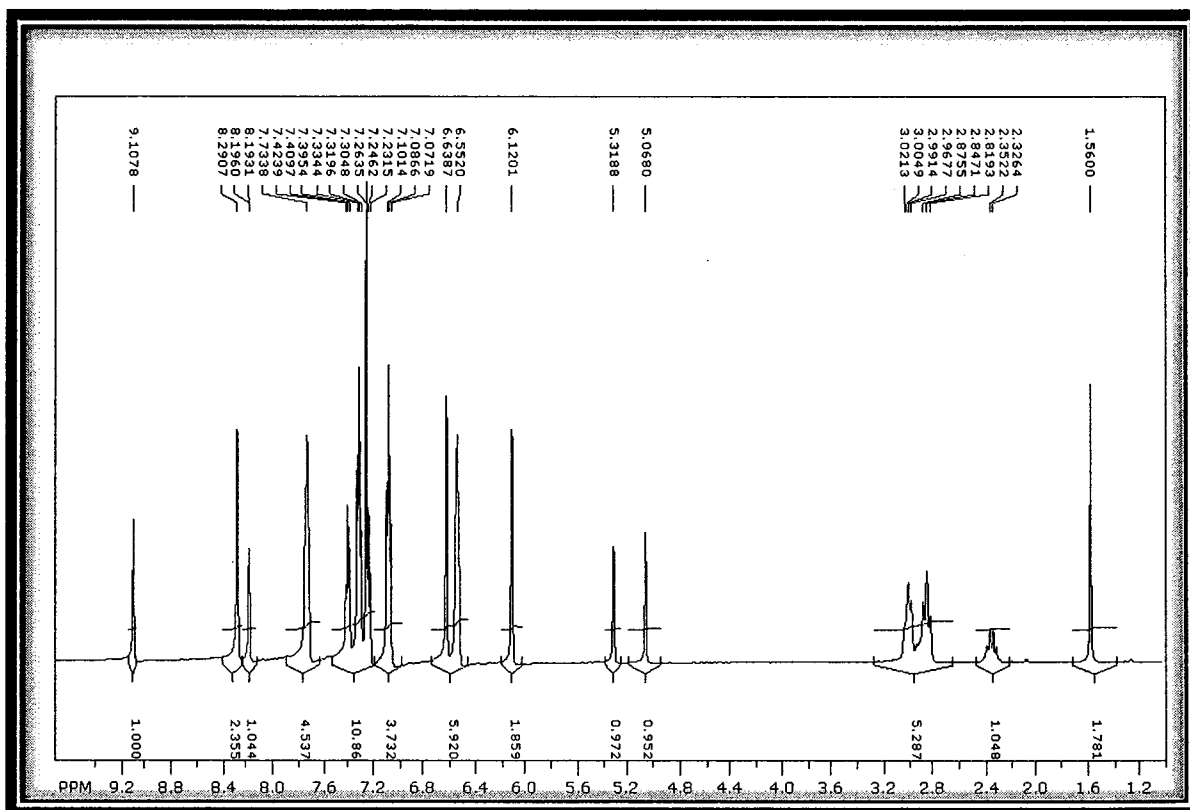water of hydration and produced values in agreement to experimental data.

Figure 17. Proton NMR spectrum of complex 7 (the signal at 1.56 ppm results from H_2O).

Single crystals of complex **7**, suitable for X-ray crystallography, were

obtained by the slow diffusion of ether into a CH_2Cl_2 solution of the complex. The

X-ray crystal structure of **7**, as illustrated in Figure 18, confirmed the proposed C_s

symmetric structure of the compounds. The ruthenium centre of compound **7**

assumes an approximately octahedral geometry with the tpm ligand occupying

one face of the octahedron and the chelating dppp and chloride ligands

completing the coordination sphere.

The bond distances observed for complex **7** between the ruthenium centre and the tpm nitrogen atoms of the pyrazole rings are similar to those observed in the structure of complex **6** [64]. Furthermore, asymmetry is observed for these
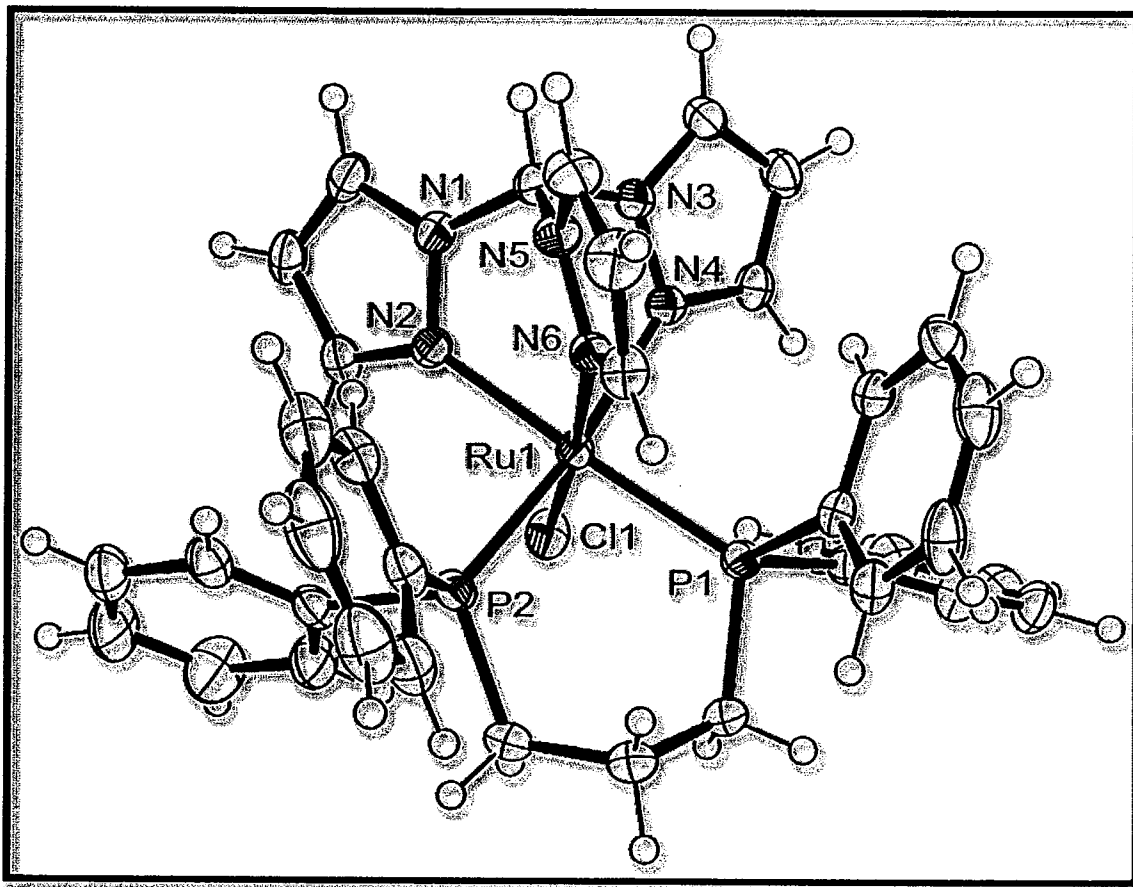
Figure 18. ORTEP drawing of complex **7**. The PF_6^- anion has been omitted for clarity. Selected bond lengths (Å) and angles (°): Ru(1)-N(6), 2.095(3); Ru(1)-N(2), 2.124(3); Ru(1)-N(4), 2.197(3); Ru(1)-P(2), 2.3035(9); Ru(1)-P(1), 2.3235(9); Ru(1)-Cl(1), 2.4056(8); N(2)-Ru(1)-N(4), 82.22(10); N(6)-Ru(1)-N(4), 82.67(10); N(6)-Ru(1)-N(2), 87.44(10); N(2)-Ru(1)-P(1), 174.43(8); N(4)-Ru(1)-P(2), 172.12(8); N(6)-Ru(1)-Cl(1), 173.59(8); P(2)-Ru(1)-P(1), 93.58(3).

same bonds, with the longer bond lengths belonging to the pyrazole nitrogens *trans* to the phosphorus atoms of the dppp ligand. This observation is attributed to the greater *trans* influence of the phosphine ligand compared to that of the chloride ligand located opposite the pyrazole nitrogen with the shorter distance from the ruthenium centre [64].

The restricted "bite" of the tpm ligand is revealed by the N-Ru-N bond angles (82.22(10)°, 82.67(10)° and 87.44(10)°), which are all less than the expected 90° angles for ideal octahedral geometry. This feature is also present in the structure of complex **6** [64]. Conversely, the P-Ru-P bond angle is greater than 90° (93.58(3)°) resulting from the three methylene spacers of the dppp ligand. As expected, removal of one of the methylene groups consequently decreases the P-Ru-P bond angle to 84.46(11)° [64]. However, the absence of the methylene spacers in the analogous bis(triphenylphosphine) complex, [(κ^3-tpm)RuCl(PPh$_3$)$_2$]PF$_6$, allows for the phosphorus atoms to adopt a more prominent obtuse angle (103.9(1)°), most likely resulting from the steric interference of the phenyl groups located on the phosphine ligands [75].

4.4 Attempted Synthesis of Diamine Complexes 9 and 10

Unfortunately, time restrictions prevented the thorough attempts to synthesize [(κ^3- tpm)RuCl(en)]PF$_6$ (**9**) and [(κ^3- tpm)RuCl(dab)]PF$_6$ (**10**) (where en= ethylenediamine and dab= 1,2-diaminobenzene). Although many attempts to synthesize these complexes were investigated, not all possible routes to their

formation were likely explored. However, experimentation with the ethylenediamine and 1,2-diaminobenzene ligands in various methods aimed at the synthesis of **9** and **10** led to some interesting observations.

4.4.1 Methods Utilizing Zinc as a Reducing Agent

Although success was met with the zinc reduction reactions in the preparation of the aforementioned solvento, phosphite and phosphine compounds, the same achievements were not realized for compounds **9** and **10** under the experimental conditions explored. The methanolic zinc reduction procedure involving en and dab did result in the formation of tpm-containing compounds as the major products; however, pure compounds could not be obtained despite employing a variety of purification techniques.

The dab ligand produced a product that was an intense burgandy-red in colour, whereas the en ligand produced a red-brown product, indicating that chemical transformations did take place. Two sets of doublets in the proton NMR spectrum of the product from the dab reaction were present downfield (7.5 - 7.0 ppm in acetone-d_6) of free dab. These signals are similar to other complexes containing chelating dab and suggest the presence of a complex containing this ligand bound to the metal with a bidentate coordination [48]. Furthermore, four broad multiplets in the proton NMR of the en reaction resonating between 7.5 – 3.9 ppm (D_2O) with a collective integration of approximately eight protons suggest the possible formation of complex [(κ^3- tpm)RuCl(en)]PF$_6$ **9**. Broad multiplets are observed in the proton NMR spectrum of similar compounds

containing en [46, 48]. However, these results remain inconclusive, and further efforts regarding purification and structural data acquisition (2D-NMR, X-ray crystallography) are required to convey confidently the formation of **9** and **10**.

4.4.2 Methods Utilizing NEt$_3$ as a Reducing Agent

There are a number of preparations cited in the literature which exploit NEt$_3$ as a reducing agent for the reduction of (κ^3-tpm)RuCl$_3$·1.5H$_2$O to produce complexes with nitrogen donating auxiliary ligands such as bipyridine and phenanthroline [62]. In light of these methods, we decided to experiment with reactions utilizing NEt$_3$ to reduce (κ^3-tpm)RuCl$_3$·1.5H$_2$O, in the presence of either en or dab, as a means to synthesize our target compounds **9** and **10**.

One reaction involving (κ^3-tpm)RuCl$_3$·1.5H$_2$O, NEt$_3$ and en proved to be rather intriguing. When the ruthenium complex was suspended in toluene and the mixture is heated to 120 °C in the presence of excess NEt$_3$ and en, a dark coloured residue coagulated on the bottom of the flask. Even though a multitude of peaks were present throughout, the proton NMR spectrum of the crude product was promising due to the fact that it contained broad multiplets that are characteristic of chelating en [46,48].

When the conditions of the reaction were optimized, a clean proton NMR spectrum of the product of interest was obtained (Figure 19). Interestingly, a similar pattern of tpm signals was present downfield as observed for complexes
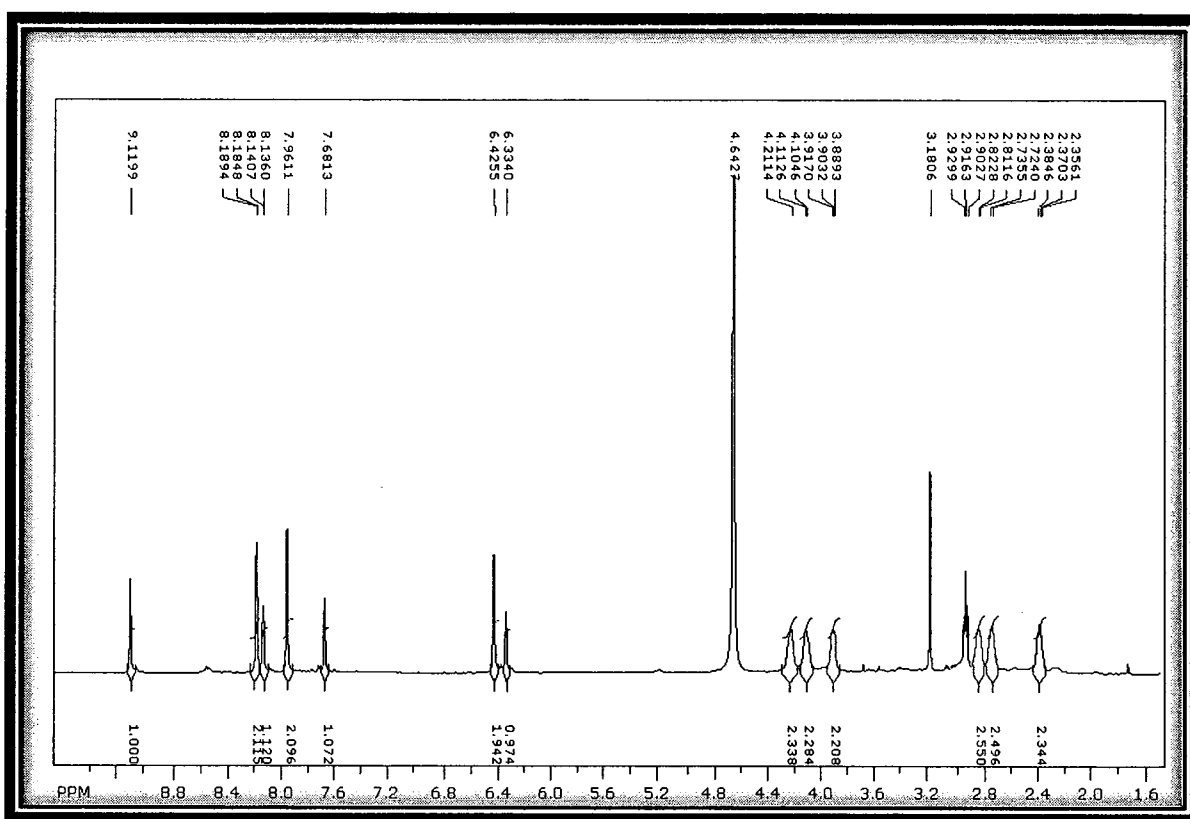
Figure 19. Proton NMR of the product obtained by the NEt$_3$ reduction reaction using en.

1-8, suggesting a structure of C$_s$ symmetry. At first glance, the signature in the upfield region of the proton NMR spectrum resembled similar ruthenium-en complexes, however the integration was different from what one would expect. The integration of the multiplets resonating between 4.3-2.3 ppm in the proton NMR spectrum revealed that each signal was a result of two protons with respect to the bridgehead proton signal of the tpm ligand. The total of 12 protons could be explained by the formation of a compound that had two ruthenium-tpm centres with each containing a chelating en ligand, and were bridged by an additional en ligand (Figure 20). Such a structure could possibly give rise to six signals each with an individual integration of two protons with respect to the

apical tpm proton signal. Although it is certainly plausible, additional evidence will be required in order to confirm this proposed structure.
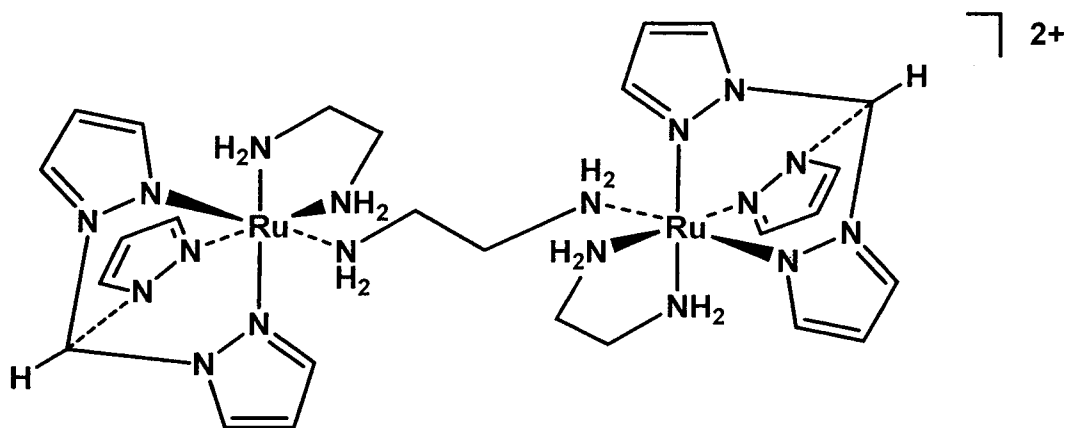
Figure 20. Proposed molecular structure of the product obtained by the NEt$_3$ reduction reaction using en.

Unfortunately, extending the NEt$_3$ reduction reactions to include the dab ligand resulted in unappealing proton NMR spectra. In each case, the pyrazole region was crowded with many peaks of varying intensities indicating that a large number of complexes were present. Purification attempts proved futile, and the reaction has been abandoned for the time being.

4.4.2 Methods Involving Complexes 1 and 2 as Precursors

Next, efforts towards synthesizing the target complexes [(κ^3-tpm)RuCl(en)]PF$_6$ **9** and [(κ^3- tpm)RuCl(dab)]PF$_6$ **10** using the solvento complexes [(κ^3- tpm)RuCl(MeCN)$_2$]PF$_6$ **1** and [(κ^3- tpm)RuCl(DMSO)$_2$]PF$_6$ **2** as precursors were explored. A great deal of experimentation was performed

including the variation of such conditions as reaction time, solvent, temperature, and reagent concentrations. In most reactions using the dab ligand, an intense burgundy-red solid was obtained. However, the proton NMR spectra were inconclusive and contained a multitude of peaks both in the pyrazole region and upfield regions of the spectra.

Attempted ligand substitution reactions involving the complex [(κ^3-tpm)RuCl(DMSO)$_2$]PF$_6$ and en, under forcing conditions (reflux in chlorobenzene at 140 °C), resulted in a product with the same proton NMR signature as that of the precursor, however, the apical tpm proton signal was absent. The reasoning behind the missing signal was not pursued. One possibility may be due to the removal of the bridgehead proton by en (and likely substituted with another non-hydrogen containing group, or possibly deuterium), but this is speculation due to the fact that deprotonation of this nature was not generally observed in this project.

These reactions put into question the lability of the DMSO ligands. Indeed, we observed that the DMSO ligands could be replaced by dppe forming complex **6**, as confirmed from phosphorus and proton NMR data, but only under forcing conditions (reflux in chlorobenzene at 140 °C). However, under these same conditions, the en did not replace the DMSO ligands; similar observations were noted with reactions involving en and complex **2**.

Attempts to synthesize complex [(κ^3- tpm)RuCl(en)]PF$_6$ (**9**) from the solvento complex [(κ^3- tpm)RuCl(MeCN)$_2$]PF$_6$ (**1**) by substituting the acetonitrile ligands by en produced interesting results. It was found that, under the same

forcing conditions that led to the replacement of the DMSO ligands by dppe, the

reaction of complex **1** with excess en resulted in the formation of product that had

a similar proton NMR spectrum (Figure 21) to the product formed during the

reaction involving NEt₃ as a reducing agent and en mentioned in the previous

section (Figure 19). Although direct comparison is difficult due to different
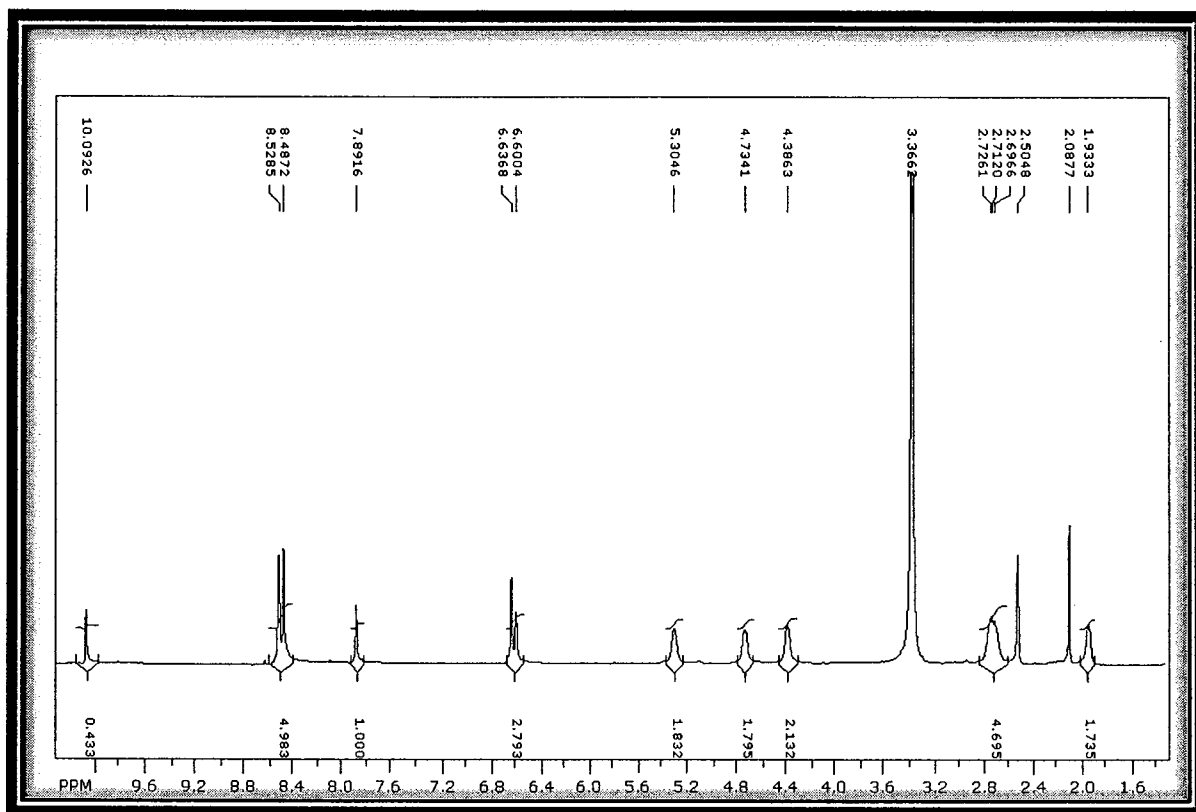
Figure 21. Proton NMR spectrum of the product formed by the reaction
[(κ³- tpm)RuCl(MeCN)₂]PF₆ and en.

deuterated solvents used in the NMR experiments, the proton NMR spectra of

these two products are similar and suggest they might be structurally similar (see

Figure 19). Similarities between the proton NMR spectra of these two products

are the presence of a set of C_s symmetric tpm signals integrating to ten protons

71

and multiplets integrating to twelve protons. Although only five multiplets were observed for the product of the reaction involving complex **1** and en (as opposed to six multiplet signals resulting from the previous NEt_3 reduction reaction), one of the multiplet signals integrates to four protons and may be a result of two overlapping signals. Unfortunately, time restrictions have delayed further investigation of this reaction, and preliminary results are inconclusive as to whether the products of these two reactions are identical.

4.5 Anticancer Activity of Complexes 1-8

Complexes **1-8** were screened for antiproliferative activity in the MCF-7 and Hela cancer cell lines using the MTT assay. The growth inhibition curves (Appendix A) display the wide range of activity of these complexes as illustrated by their inhibitory concentrations listed in Table 2. Since inhibitory concentrations vary considerably with the conditions and cell lines that are used in their determination, comparison with other relevant complexes reported in the literature is difficult. Therefore, it was decided to determine the inhibitory concentrations for $[(\eta^6$-p-cymene)RuCl(κ^2-dppp)]Cl (*vide infra*), *cisplatin* and doxorubicin under the same experimental conditions as used for complexes **1-8** for direct comparison. These values are also listed in Table 2.

Although solvento compounds **1-2** were not included as specified target compounds for anticancer investigations, it was decided to test these compounds to see if they had any effect on cell proliferation. Unfortunately, and maybe not

surprisingly, these two complexes did not display significant antiproliferative activities as revealed by their inhibitory concentrations exceeding the maximum concentrations tested (> 20 µM and > 50 µM for **1** and **2** respectively). One possible reason, as proposed by Sadler for analogous ruthenium-arene compounds [25], is that these complexes may become deactivated by components in the cell or cell media resulting in insignificant antiproliferative activity. Alternatively, given the limited lability of the solvent ligands in past reactions with en, dap, dppe and complexes **1** and **2,** it is possible that these complexes are unable to interact with biochemical targets and, thus, are incapable of inducing cell cycle arrest and/or apoptosis.

Interestingly, complex **3** displayed moderate anticancer activity displayed by its inhibitory concentration of 32.1 and 40.4 µM in the MCF-7 and Hela cells, respectively. This moderate activity is promising, and suggests future studies of a variety of phosphite ligands in order to determine if similar complexes bearing phosphite ligands can improve upon this antiproliferative activity. It would also prove interesting to see if the mode of action of complex **3** was similar to the hypothetical mode of action that was the inspiration (stabilized DNA interaction via hydrogen bonding between the oxygen atom of the phosphite ligand and the exocyclic amino hydrogen atoms of the adenine nucleobase) to include this complex among the target compounds of this project.

Table 2. Growth inhibition of MCF-7 (breast) and HeLa (cervical) cancer cells after exposure to complexes **1-6**, [(η^6-p-cymene)RuCl(κ^2-dppp)]Cl, cisplatin and doxorubicin.

Compound	IC$_{50}$ (µM)	
	MCF-7	HeLa
1	> 20	NA
2	> 50	> 50
3	32.1 ± 3.39	40.4 ± 5.52
4	4.7 ± 0.07	7.4 ± 0.21
5	11.6 ± 0.14	9.5 ± 1.9
5 (recrystallized)	47 ± 0.71	> 50
6	8.1 ± 0.46	4.0 ± 0.00
7	2.9 ± 0.07	6.9 ± 1.31
8	2.9 ± 0.07	5.8 ± 0.35
[(η^6-p-cymene)RuCl(κ^2-dppp)]Cl	0.8 ± 0.00	1.4 ± 0.07
cisplatin	> 18	12.4 ± 0.85
doxorubicin	0.7 ± 0.2	1.0 ± 0.2

One very puzzling aspect of this project concerned the MTT assay results of complex **5**. Early in the development of extending the zinc reduction reaction to include the dppm ligand, a product was isolated that displayed a single phosphorus NMR signal (in addition to PF$_6^-$). However, the proton NMR spectrum showed that the product was not completely pure due to the presence of small

broad signals in the phenyl and upfield regions of the spectrum. Another

indication that the product was not pure was that it appeared green-yellow as

opposed to the bright yellow of the rigorously pure compound. The impure

compound was tested to see if there were any prospects of antiproliferative

activity. Interestingly, the green-yellow product displayed growth inhibitory

properties with an IC_{50} of 11.6 and 9.5 µM in MCF-7 and Hela cancer cells,

respectively. This activity is quite remarkable considering *cisplatin* has an IC_{50} of

18.4 and 12.4 µM in MCF-7 and Hela cell lines, respectively (Table 2).

Interestingly, rigorously purified **5** lost its inhibitory properties and had IC_{50} of 47

and > 50 µM for MCF-7 and Hela cells, respectively. In separate tests it was

established that the MTT reagent had not been compromised and thus was ruled

out as the source of the differing results.

Three possible scenarios that which might explain the conflicting data

include an impurity with anticancer properties, a false positive, or a negative

result. The impurity in the preliminary sample that was tested may have been a

potent anticancer compound that had remarkable activity even at a low

concentration. There is a possibility that the impurity together with complex **5**

synergistically produced a cytotoxic effect. Purification would remove the impurity

and the synergistic effect would be lost. Conversely, the first set of results

obtained for the impure sample of complex **5** may have been false positives, and

a problem with the testing of this sample may have been the cause of this

confusion. An unforeseen problem, besides the validity of the MTT reagent, may

have occurred during testing the pure compound; however, this is unlikely due to

the fact that the tests performed with this compound were performed in quadruplicate. It is interesting to note the remarkable activity that was discovered for rigorously pure compounds **4** and **6-8**, all of which are structurally very similar to complex **5**.

Among the most exciting outcomes of this project were the anticancer properties of compounds **4** and **6-8.** These complexes revealed extraordinary antiproliferative effects as evidenced by their inhibitory concentrations all below 8.2 µM for both cell lines. Although each complex was more active than cisplatin, complex **8** was the most active with IC_{50} six times lower than that of cisplatin in MCF-7 cells and two times more active than cisplatin on the Hela cell line. Their cytotoxicities were comparable to that of doxorubicin, another commonly-used anticancer drug, as their IC_{50} values were within one log of each other. Compounds **4** and **6-8** were more active towards the MCF-7 breast cancer cell line as compared to the Hela cervical cancer cell line except for complex **6** whose activity revealed the opposite trend. Additional investigation regarding the mode of action of these complexes will be needed in order to explain these observations.

The MTT assay measures the activity of mitochondrial dehydrogenase, which reflects the viability of the cells. However, since the effects of the compounds were measured against untreated control cells that continue to grow, a decline in MTT reading in the treated cells may also be seen if a certain compound has cytostatic properties. Since these treated cells are prevented from multiplying while the untreated controls continue to grow, the lower MTT readings

of the treated cells may be mistaken for cell killing. However, the fold difference can give an indication of whether the effect is cytostatic or cytotoxic. In the situation whereby the compounds were cytostatic, the cells would still be viable with intact mitochondria and would produce relatively high MTT readings that might only be several fold lower than the untreated controls. This would depend on how fast the untreated cells grew in the 72 hr period of treatment. However, if the treated cells showed very low readings of about 10% or less of the controls, as seen with compound **4-8**, that would be highly indicative of cell killing as there were less cells remaining in the wells than were initially seeded. Other assays would then have to be performed to determine if the compounds induced apoptosis or necrosis, or a mixture of both. For clinical purposes, agents that induce apoptosis are generally preferred since the cellular contents remain contained until the cellular remnants get phagocytized. Necrotic cell death usually results in the rupture of the cell membrane and the release of cellular contents. Besides cellular structures, the released contents would include degradative enzymes that would be detrimental to the surrounding cells, leading to an accumulation of dead tissues and debris. These necrotic tissues may then need to be surgically removed.

The intent of testing compounds **4** and **6-8** was to determine if the size of the alkyl chain affects the anticancer properties of these compounds. Complex **4** was included as the closest related compound that lacked an alkyl linkage between the two phosphorus atoms. Since the activities of these phosphine compounds are very similar and a definite trend in their activity is absent, it is

difficult to say if the alkyl chain has much of an effect on the anticancer properties of these compounds. Further studies centered on structure-activity relationships and the mode of action of these compounds will aid in the explanation of the antiproliferative activity displayed by compounds **4** and **6-8**.

The piano stool complex [(η^6-p-cymene)RuCl(κ^2-dppp)]Cl was tested for anticancer properties for comparative purposes to try and establish the role of the tpm ligand of our target compounds [63]. To our amazement, the activity of this compound was much greater than that of cisplatin in both cell lines. Astonishingly, the antiproliferative activity of this compound is close to that of the anticancer compound doxorubicin in both the MCF-7 and Hela cancer cell lines. However, there is not a substantial difference in the activity of this compound as compared to the analogous tpm-containing compound **7**. Thus, conclusions regarding the role of the tpm ligand in the anticancer activity of compounds **3-8** remain ambiguous and further studies are required.

4.6 Concluding Remarks

A convenient synthetic route to a variety of tpm-ruthenium(II) compounds was discovered utilizing Zn dust as a reducing agent for (κ^3-tpm)RuCl$_3$·1.5H$_2$O. The versatility of this method is exemplified by the variety of auxiliary ligands that have been used in the synthesis of our target compounds including solvent ligands, monodentate phosphine and phosphite ligands and a number of bis(diphenylphosphino)alkanes. Unfortunately, time restrictions hindered the

investigation of the applicability of the ligands ethylenediamine and 1,2-diaminobenzene in this Zn reduction reaction.

Similar results were obtained for the reaction utilizing NEt_3 as a reducing agent for $(\kappa^3\text{-tpm})RuCl_3 \cdot 1.5H_2O$ and the attempted ligand substitution reaction the complex $[(\kappa^3\text{- tpm})RuCl(MeCN)_2]PF_6$, both involving en. The similarities between the proton NMR spectra of products of these reactions provide evidence that the same compound is formed in both reactions. The proposed structure of this compound can be described as a dinuclear tpm-ruthenium(II) compound containing a bridging en ligand and two chelating en ligands. However, further study is required to confirm if these products are identical and if the proper structure has been proposed.

Although solvento complexes **1** and **2** were not active against MCF-7 and Hela cells, it must be kept in mind that that these compounds could be active against metastases. NAMI-A and many of the RAPTA-type complexes failed to produce significant inhibitory concentrations, in the first line of testing, using the MTT assays [4,34,43,76]. It was not until these compounds were tested by other means that their antimetastatic activities were revealed. In addition, these two solvento compounds may also serve as useful precursors in the synthesis of other tpm-ruthenium complexes.

The moderate activity of complex **3** containing the phosphite ligands is promising and should not be regarded as a failed prospect. Some of the compounds developed by Sadler, for example, revealed only moderate activity, and only when these structures were optimized did their true potential come to

light [46,48]. Variation of the phosphite ligand may produce compounds that have remarkable anticancer activity.

It is quite exciting to synthesize compounds that have not been studied in the past, and to be able to gather interesting structural information including X-ray diffraction data. This excitement is amplified to exhilaration when such compounds are found to have interesting preliminary effects on a devastating disease such as cancer. This project was a prime example of excitement reaching exhilaration as a result of the remarkable anticancer activity that the phosphine compounds studied in this project displayed against two common tumour models. The findings presented in this study suggest further investigation of these and related compounds to elucidate structure-activity relationships, details regarding their mode(s) of action and their potential as chemotherapeutic treatments for cancer patients.

4.7 Future Prospects

Undoubtedly, this project forms a solid stem from which many branches of explorations could originate. The following section will briefly mention only a small fraction of the possible directions one could investigate as a continuation of this project.

One of the main reasons that the tpm ligand was included in the molecular design was its versatility. Because of time constraints, functionalization of the tpm ligand was one of the areas of the project that was not explored.

Manipulation of the tpm ligand to fine-tune the activity and/or the aqueous solubility of the anticancer compounds could lead to compounds with enhanced anticancer properties and ones that are better fit for use in a clinical setting (i.e. water solubility for administering the drug or compounds that could be taken orally). Furthermore, the integration of biologically relevant moieties (such as human serum albumin or estrogen) may provide a means to make these compounds more targeted towards cancer cells.

Ligand variation is another area that will be studied. The screening of compounds with different phosphines and phosphite ligands is sure to lead to the discovery of additional novel anticancer compounds. The incorporation of water-soluble phosphine ligands may impart water solubility to their coordination compounds and may be employed to balance the hydrophobic/hydrophilic nature of these complexes. Experimentation with bridging ligands and the formation of multinuclear phosphine compounds may also be an interesting route to complexes that display interesting anticancer activity.

Insight into the solution chemistry of ruthenium anticancer compounds is also an important aspect. The determination of whether or not these compounds experience aquation under physiological conditions may provide details regarding their mode of action. In addition, replacement of the chloride ligands with other labile or non-labile ligands might serve as a simple method to modify these complexes and adjust their anticancer activity.

Although these are just a small indication of the possible directions that could be investigated, there are a number of chemical and biological studies that

could provide interesting information regarding ruthenium-phosphine anticancer compounds. Intriguing studies are sure to follow, for it will be these future research initiatives that determine the true value of these potential chemotherapeutic agents.

References

1. M.J. Clarke, *Coord. Chem. Rev.*, 2003, **236**, 209.
2. E. Reisner, V.B. Arion, B.K. Keppler and A.J.L. Pombeiro, *Inorg. Chim. Acta.*, 2008, **361**,1569.
3. C.S. Allardyce and P.J. Dyson, *Top. Organomet. Chem.*, 2006, **17**, 177.
4. M.J. Hannon, *Pure Appl. Chem.*, 2007, **79**, 2243.
5. H. Zorbas and B.K. Keppler, *ChemBioChem.*, 2005, **6**, 1157.
6. J. Reedijk, *Eur. J. Inorg. Chem.*, 2009, **10**, 1303.
7. E. Wong and C.M. Giandomenico, *Chem. Rev.*, 1999, **99**, 2451.
8. P.J. Dyson and G. Sava, *Dalton Trans.*, 2006,**16**,1929.
9. G. Chu, *J. Bio. Chem.*,1994, **269**, 787.
10. Z.H. Siddik*, Oncogene*, 2003, **22**, 7265.
11. P. Jordan and M. Carmo-Fonseca, *Cell. Mol. Life Sci.*, 2000, 57, 1229.
12. C. X. Zhang and S.J. Lippard, *Curr. Opin. Chem. Biol.*, 2003, **7**, 481.□
13. A.M. Di Francesco, A. Ruggiero and R. Riccardi, *Cell. Mol. Life Sci.*, 2002, **59**, 1914,
14. S.J. Berners-Price and P.J. Sadler, Bioinorganic Chemistry, Springer Berlin/ Heidelberg, 1988, 27.
15. W. F. Kean, L. Hart and W. W. Buchanan, *Br. J. Rheumatol.*, 1997, **36**, 560.
16. C.K. Mirabelli, R.K. Johnson, C. M. Sung, L. Faucette, K. Muirhead and S.T. Crooke, *Cancer Res.*,1985, **45**, 32.
17. M.J. McKeage, L. Maharaj and S.J. Berners-Price, *Coord. Chem. Rev.,* 2002, **232**,127.
18. P.J. Barnard and S.J. Berners-Price. *Coord. Chem. Rev.,* 2007, 251, 1889.
19. C.K. Mirabelli, R.K. Johnson, D.T. Hill, L.F. Faucette, G.R. Girard, G.Y. Kuo, C. M. Sung and S.T. Crooke, *J. Med. Chem.*, 1986, **29**, 218.
20. S.J. Berners-Price, C.K. Mirabelli, R.K. Johnson, M.R. Mattern, F.L. McCabe, L.F. Faucette, C.-M. Sung, S.-M. Mong, P.J. Sadler and S.T. Crooke, *Cancer Res.*, 1986, **46**, 5486.
21. S.J. Berners-Price, G.R. Girard, D.T. Hill, B.M. Sutton, P.S. Jarrett, L.F. Faucette, R.K. Johnson, C.K. Mirabelli and P.J. Sadler, *J. Med. Chem.*, 1990, **33**, 1386.
22. N.J. Sanghamitra, P. Phatak, S. Das, A.G. Samuelson and K. Somasundaram, *J. Med. Chem.*, 2005, **48**, 977.
23. E. Reisner, V.B. Arion, B.K. Keppler and A.J.L. Pombeiro, *Inorg. Chim. Acta*, 2008, **361**, 1569.
24. H. Sun, H. Li and P.J. Sadler, *Chem. Rev.*, 1999, **99**, 2817.
25. Y.K. Yan, M. Melchart, A. Habtemariam and P.J. Sadler, *Chem. Commun.*, 2005, **39**, 4764.
26. G. Sava, S. Pacor, G. Mestroni and E. Alessio, *Clin. Exp. Metastasis,* 1992, **10**, 273.
27. E. Germanov, J.N. Berman and D.L Guernsey, *Int. J. Mol. Med.,* 2006, **18**, 1025.
28. D. Griffith, S. Cecco, E. Zangrando, A. Bergamo, G. Sava and C.J. Marmion, *J. Biol. Inorg. Chem.*, 2008,**13**, 511.

29. M. Bacac, A.C.G. Hotze, K. van der Schilden, J.G. Haasnoot, S. Pacor, E. Alessio , G. Sava and J. Reedijk, *J. Inorg. Biochem.*, 2004, **98**, 402.

30. C. Moucheron, *New J. Chem.*, 2009, **33**, 235.

31. J.M. Rademaker-Lakhai, D. van den Bongard, D. Pluim, J.H. Beijnen and J.H.M. Schellens. *Clin. Cancer Res.*, 2004, **10**, 3717.

32. C.G. Hartinger, S. Zorbas-Seifried, M.A. Jakupec, B. Kynast, H. Zorbas and B.K. Keppler, *J. Inorg. Biochem.*, 2006, **100**, 891.

33. C.G. Hartinger, M.A. Jakupec, S. Zorbas-Seifried, M Groessl, A. Egger, W. Berger, H. Zorbas, P.J. Dyson and B.K. Keppler, *Chem. & Biodiv.*, 2008, **5**, 2140.

34. C.Scolaro, A. Bergamo, L. Brescacin, R. Delfino, M. Cocchietto, G. Laurenczy, T.J. Geldbach, G. Sava and P.J. Dyson, *J. Med. Chem.*, 2005, **48**, 4161.

35. C.S. Allardyce, P.J. Dyson, D.J. Ellis and S.L. Heath, *Chem. Commun.*, 2001, **15**, 1396.

36. A.D. Phillips, L. Gonsalvi, A. Romerosa, F. Vizza and M. Peruzzini, *Coord. Chem. Rev.*, 2004, **248**, 955.

37. C.G. Hartinger and P.J. Dyson, *Chem. Soc. Rev.*, 2009, **38**, 391.

38. S. Chatterjee, S. Kundu, A. Bhattacharyya, C.G. Hartinger and P.J. Dyson, *J. Biol. Inorg.* Chem. 2008, 13, 114.

39. C. Scolaro, C.G. Hartinger, C.S. Allardyce, B.K. Keppler and P.J. Dyson, *J. Inorg. Biochem.*, 2008,**102**, 1743.

40. A. Casini, G. Mastrobuoni, W.H. Ang, C. Gabbiani, G. Pieraccini, G. Moneti, P.J. Dyson and L. Messori, *ChemMedChem.* 2007, **2**, 631.

41. A. Casini, C. Gabbiani, F. Sorrentino, M.P. Rigobello, A. Bindoli, T.J. Geldbach, A. Marrone, N. Re, C.G. Hartinger, P.J. Dyson and L. Messori, *J. Med. Chem.* 2008, ***51***, 6773.

42. M.M. Mohamed and B.F. Sloane, *Nat. Rev. Cancer*, 2006, **6**, 764.

43. W.H. Ang, E. Daldini, C. Scolaro, R. Scopelliti, L. Juillerat-Jeannerat and P.J. Dyson, *Inorg.* Chem. 2006, **45**, 9006.

44. R.E. Aird, J. Cummings, A.A. Ritchie, M. Muir, R.E. Morris, H. Chen, P.J. Sadler and D.I. Jodrell, *Br. J. Cancer*, 2002, **86**, 1652.

45. F. Wang, H. Chen, S. Parsons, I.D.H. Oswald, J.E. Davidson and P.J. Sadler. *Chem. Eur. J.*, 2003, **9**, 5810.

46. R.E. Morris, R.E. Aird, P. del S. Murdoch, H. Chen, J. Cummings, N.D. Hughes, S. Parsons, A. Parkin, G. Boyd, D.I. Jodrell and P.J. Sadler, *J. Med. Chem.*, 2001, **44**, 3616.

47. H. Chen, J. A. Parkinson, S. Parsons, R.A. Coxall, R.O. Gould and P.J. Sadler, *J. Am. Chem. Soc.*, 2002, **124**, 3064.

48. A. Habtemariam, M. Melchart, R. Fernandez, S. Parsons, I.D.H. Oswald, A. Parkin, F.P.A. Fabbiani, J.E. Davidson, A. Dawson, R.E. Aird, D. I. Jodrell and P.J. Sadler, *J. Med. Chem.* 2006, **49**, 6858.

49. H. Chen, J.A. Parkinson, R.E. Morris and P.J. Sadler, *J. Am. Chem. Soc.*, 2003, 125, 173.

50. R. Fernandez, M. Melchart, A. Habtemariam, S. Parsons and P.J. Sadler, *Chem. Eur. J.*, 2004, 10, 5173.

51. M. Melchart, A. Habtemariam, S. Parsons and P.J. Sadler, *J. Inorg. Biochem.*, 2007, 101, 1903.

52. (a) C. Gossens, I. Tavernelli and U. Rothlisberger, *J. Chem. Theory Comput.*, 2007, **3**, 1212. (b) C. Gossens, I. Tavernelli and U. Rothlisberger, *J. Am. Chem. Soc.*, 2008, **130**, 10921.

53. F. Wang, A. Habtemariam, E.P.L. van der Geer, R. Fernandez, M. Melchart, R.J. Deeth, R. Aird, S. Guichard, F.P.A. Fabbiani, P. Lozano-Casal, I.D.H. Oswald, D.I. Jodrell, S. Parsons and P.J. Sadler, *Proc. Natl. Acad. Sci. USA*, 2005, **102**, 18269.

54. M.H. Garcia, T.S. Morais, P Florindo, M.F.M. Piedade, V. Moreno, C. Ciudad and V. Noe, *J. Inorg. Biochem.*, 2009, **103**, 354.

55. L.A. Huxham, E.L.S. Cheu, B.O. Patrick and B.R. James, *Inorg. Chim. Acta*, 2003, **352**, 238.

56. J. Carmichael, W.G. DeGraff, A.F. Gazdar, J.D. Minna and J.B. Mitchell, *Cancer Res.*, 1987, **47**, 936.

57. S.P.C. Cole, *Cancer Chemother. Pharmacol.*, 1986, **17**, 259.

58. S. Ahmadian, J. Barar, A.A. Saei, M.A.A. Fakhree and Y. Omidi. *J. Vis. Exp.*, 2009, **26**.

59. D.L. Reger, T.C Grattan, K.J. Brown, C.A. Little, J.J.S. Lamba, A.L. Rheingold and R.D. Sommer, *J. Organomet. Chem.*, 2000, **607**, 120.

60. W. Kläui, M. Berghahn, G. Rheinwald and H. Lang, *Angew. Chem. Int. Ed.*, 2000, **39**, 2464.

61. A.B. Pangborn, M.A. Giardello, R.H. Grubbs, R.K. Rosen and F.J. Timmers, *Organometallics*, 1996, **15**, 1518.

62. A. Llobet, P. Doppelt and T.J. Meyer, *Inorg. Chem.*, 1988, **27**, 514.

63. C. Daguenet, R. Scopelliti and P.J. Dyson, *Organometallics*, 2004, **23**, 4849.

64. D.C. Wilson and J.H. Nelson, *J. Organomet. Chem.*, 2003, **682**, 272.

65. APEX2 (Version 2.0-2, 2006), SAINT (Version 7.23A, 2005), XPREP (Version 2005/2, 2005) and SHELXTL (Version 6.14, 2000) software for CCD diffractometers, Bruker AXS Inc., Madison, WI, USA.

66. D.T. Cromer and J.T. Waber, International Tables for X-ray Crystallography, Kynoch Press: Birmingham, UK, 1974; vol. 4, Table 2.2A.

67. $R_1 = \sum ||F_o| - |F_c|| / \sum |F_o|$

$wR_2 = \{\sum[w (F_o^2 - F_c^2)^2] / \sum[w(F_o^2)^2]\}^{\frac{1}{2}}$

$(w = 1 / [\sigma^2(F_o^2) + (0.0456P)^2 + 6.7266P]$, where $P = [Max (F_o^2, 0) + 2F_c^2] / 3)$

68. L.J. Farrugia, *J. Appl. Cryst.*, 1997, **30**, 565.

69. J. Carmichael, W.G. DeGraff, A.F. Gazdar, J.D. Minna and J.B. Mitchell, *Cancer Res.*, 1987, **47**, 936.

70. M. Yamaguchi, T. Iida and T. Yamagishi, *Inorg. Chem. Commun.*, 1998, **1**, 299.

71. (a) C. Slugovc, C. Gemel, J.Y. Shen, D. Doberer, R. Schmid, K. Kirchner and K. Mereiter, *Monatshefte für Chemie.* 2000, **130**, 1241. (b) E. Rüba, W. Simanko, K. Mauthner, K.M. Soldouzi, C. Slugovc, K. Mereiter, R. Schmid

and Karl Kirchner, *Organometallics*, 1999, **18**, 3843.

72. E. Iengo, E. Zangrando, E. Baiutti, F. Munini and E. Alessio, *Eur. J. Inorg. Chem.* 2005, 1019.

73. L.L. Romualdo, A.L. Bogado, E.M.A. Valle, I.S. Moreira, J. Ellena, E.E. Castellano, M.P. de Araujo and A.A. Batista, *Polyhedron*, 2008, **27**, 53.

74. (a) S. Doherty, J.G. Knight, R.K. Rath, W. Clegg, R.W. Harrington, C.R. Newman, R. Campbell and H. Amin, *Organometallics*, 2005, **24**, 2633; (b) D.E. Fogg and B.R. James, *J. Organomet. Chem.*, 1993, **462**, C21.

75. L.D. Field, B.A. Messerle, L. Soler, I.E. Buys and T.W. Hambley, *J. Chem. Soc., Dalton Trans.*, 2001, 1959.

76. A.H. Velders, A. Bergamo, E. Alessio, E. Zangrando, J.G. Haasnoot, C. Casarsa, M. Cocchietto, S. Zorzet and G. Sava, *J. Med. Chem.*, 2004, **47**, 1110.

Appendix A. Growth Inhibition Curves

MCF-7 Cancer Cells Exposed to [(κ^3- tpm)RuCl(MeCN)$_2$][PF$_6$] (1)

Absorbance *vs* Concentration of [(κ^3- tpm)RuCl(MeCN)$_2$][PF$_6$] for MCF-7 Cells (Trial 1)

IC$_{50}$ = >20 µM

Concentration of [(κ^3- tpm)RuCl(MeCN)$_2$][PF$_6$] (µM)

MCF-7 Cancer Cells Exposed to [(κ^3- tpm)RuCl(DMSO)$_2$][PF$_6$] (2)

Absorbance *vs* Concentration of [(κ^3- tpm)RuCl(DMSO)$_2$][PF$_6$] for MCF-7 Cells (Trial 1)

IC$_{50}$ = > 50 µM

Concentration of [(κ^3- tpm)RuCl(DMSO)$_2$][PF$_6$] (µM)

**Absorbance *vs* Concentration of [(κ³- tpm)RuCl(DMSO)₂][PF₆]
for MCF-7 Cells (Trial 2)**

IC₅₀ = > 50 µM

Concentration of [(κ³- tpm)RuCl(DMSO)₂][PF₆] (µM)

HeLa Cancer Cells Exposed to [(κ³- tpm)RuCl(DMSO)₂][PF₆] (2)

**Absorbance *vs* Concentration of [(κ³- tpm)RuCl(DMSO)₂][PF₆]
for HeLa Cells (Trial 1)**

IC₅₀ = > 50 µM

Concentration of [(κ³- tpm)RuCl(DMSO)₂][PF₆] (µM)

Absorbance *vs* Concentration of $[(\kappa^3\text{- tpm})RuCl(DMSO)_2][PF_6]$
for HeLa Cells (Trial 2)

$IC_{50} = > 50 \; \mu M$

Concentration of $[(\kappa^3\text{- tpm})RuCl(DMSO)_2][PF_6]$ (μM)

MCF-7 Cancer Cells Exposed to $[(\kappa^3\text{-tpm})RuCl(P(OMe)_3)_2][PF_6]$ (3)

Absorbance *vs* Concentration of $[(\kappa^3\text{-tpm})RuCl(P(OMe)_3)_2][PF_6]$
for MCF-7 Cells (Trial 1)

$IC_{50} = 34.5 \; \mu M$

Concentration of $[(\kappa^3\text{-tpm})RuCl(P(OMe)_3)_2][PF_6]$ (μM)

Absorbance *vs* Concentration of $[(\kappa^3\text{-tpm})RuCl(P(OMe)_3)_2][PF_6]$ for MCF-7 Cells (Trial 2)

$IC_{50} = 29.7\ \mu M$

HeLa Cancer Cells Exposed to $[(\kappa^3\text{-tpm})RuCl(P(OMe)_3)_2][PF_6]$ (3)

Absorbance *vs* Concentration of $[(\kappa^3\text{-tpm})RuCl(P(OMe)_3)_2][PF_6]$ for HeLa Cells (Trial 1)

$IC_{50} = 44.3\ \mu M$

Absorbance *vs* Concentration of $[(\kappa^3\text{-tpm})RuCl(P(OMe)_3)_2][PF_6]$ for HeLa Cells (Trial 2)

$IC_{50} = 35.6\ \mu M$

Concentration of $[(\kappa^3\text{-tpm})RuCl(P(OMe)_3)_2][PF_6]$ (µM)

MCF-7 Cancer Cells Exposed to $[(\kappa^3\text{-tpm})RuCl(PMePh_2)_2][PF_6]$ (4)

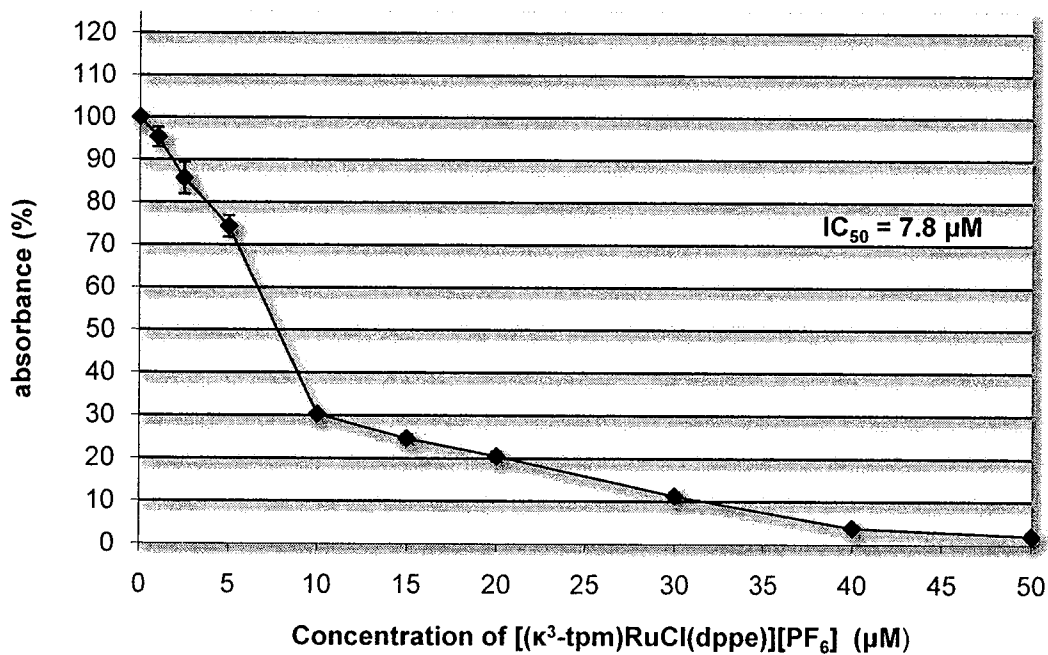### Absorbance *vs* Concentration of $[(\kappa^3\text{-tpm})RuCl(PMePh_2)_2][PF_6]$ for MCF-7 Cells (Trial 1)

$IC_{50} = 4.7\ \mu M$

Concentration of $[(\kappa^3\text{-tpm})RuCl(PMePh_2)_2][PF_6]$ (µM)

**Absorbance *vs* Concentration of [(κ³-tpm)RuCl(PMePh₂)₂][PF₆]
for MCF-7 Cells (Trial 2)**

IC$_{50}$ = 4.6 μM

absorbance (%)

Concentration of [(κ³-tpm)RuCl(PMePh₂)₂][PF₆] (μM)

HeLa Cancer Cells Exposed to [(κ³-tpm)RuCl(PMePh₂)₂][PF₆] (4)

**Absorbance *vs* Concentration of [(κ³-tpm)RuCl(PMePh₂)₂][PF₆]
for HeLa Cells (Trial 1)**

IC$_{50}$ = 7.5 μM

absorbance (%)

Concentration of [(κ³-tpm)RuCl(PMePh₂)₂][PF₆] (μM)

Absorbance *vs* Concentration of [(κ³-tpm)RuCl(PMePh₂)₂][PF₆] for HeLa Cells (Trial 2)

$IC_{50} = 7.2\mu M$

Concentration of [(κ³-tpm)RuCl(PMePh₂)₂][PF₆] (μM)

MCF-7 Cancer Cells Exposed to Impure [(κ³-tpm)RuCl(dppm)][PF₆] (5)

Absorbance *vs* Concentration of [(κ³-tpm)RuCl(dppm)][PF₆] for MCF-7 Cells (Trial 1)

$IC_{50} = 11.7 \ \mu M$

Concentration of [(κ³-tpm)RuCl(dppm)][PF₆] (μM)

Absorbance *vs* Concentration of [(κ³-tpm)RuCl(dppm)][PF₆] for MCF-7 Cells (Trial 2)

IC₅₀ = 11.5 µM

HeLa Cancer Cells Exposed to Impure [(κ³-tpm)RuCl(dppm)][PF₆] (5)

Absorbance *vs* Concentration of [(κ³-tpm)RuCl(dppm)][PF₆] for HeLa Cells (Trial 1)

IC₅₀ = 10.6 µM

94

Absorbance *vs* Concentration of [(κ³-tpm)RuCl(dppm)][PF₆]
for HeLa Cells (Trial 2)

$IC_{50} = 7.3\ \mu M$

absorbance (%)

Concentration of [(κ³-tpm)RuCl(dppm)][PF₆] (μM)

Absorbance *vs* Concentration of [(κ³-tpm)RuCl(dppm)][PF₆]
for HeLa Cells (Trial 3)

$IC_{50} = 10.7\ \mu M$
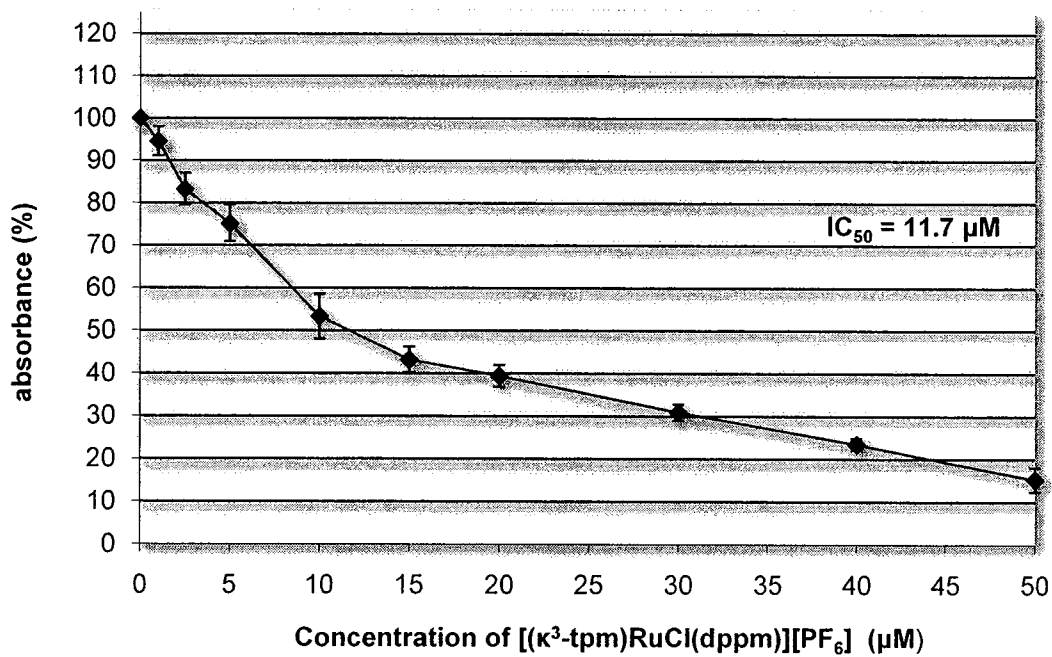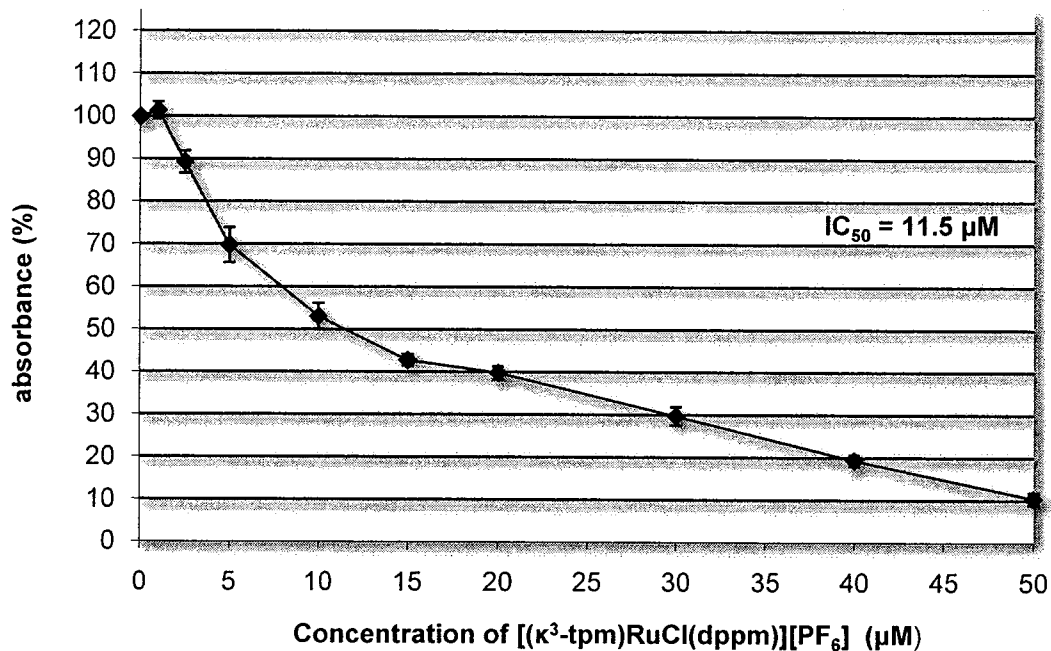
absorbance (%)

Concentration of [(κ³-tpm)RuCl(dppm)][PF₆] (μM)

MCF-7 Cancer Cells Exposed to Purified [(κ³-tpm)RuCl(dppm)][PF₆] (5)

**Absorbance *vs* Concentration of Purified [(κ³-tpm)RuCl(dppm)][PF₆]
for MCF-7 Cells (Trial 1)**

IC$_{50}$ = > 50 µM

Concentration of [(κ³-tpm)RuCl(dppm)][PF₆] (µM)

**Absorbance *vs* Concentration of Purified [(κ³-tpm)RuCl(dppm)][PF₆]
for MCF-7 Cells (Trial 2)**

IC$_{50}$ = 37.7 µM

Concentration of [(κ³-tpm)RuCl(dppm)][PF₆] (µM)

Absorbance *vs* Concentration of Purified [(κ³-tpm)RuCl(dppm)][PF₆] for MCF-7 Cells (Trial 3)

$IC_{50} = 47 \, \mu M$

absorbance (%)

Concentration of [(κ³-tpm)RuCl(dppm)][PF₆] (μM)

Absorbance *vs* Concentration of Purified [(κ³-tpm)RuCl(dppm)][PF₆] for MCF-7 Cells (Trial 4)

$IC_{50} = 46 \, \mu M$

absorbance (%)

Concentration of [(κ³-tpm)RuCl(dppm)][PF₆] (μM)

Absorbance *vs* Concentration of Purified [(κ³-tpm)RuCl(dppm)][PF₆]
for HeLa Cells (Trial 1)

IC₅₀ = > 50 µM

Concentration of [(κ³-tpm)RuCl(dppm)][PF₆] (µM)

Absorbance *vs* Concentration of Purified [(κ³-tpm)RuCl(dppm)][PF₆]
for HeLa Cells (Trial 2)

IC₅₀ = > 50 µM

Concentration of [(κ³-tpm)RuCl(dppm)][PF₆] (µM)

Absorbance *vs* Concentration of Purified [(κ³-tpm)RuCl(dppm)][PF₆] for HeLa Cells (Trial 3)

IC₅₀ = > 50 μM

Concentration of [(κ³-tpm)RuCl(dppm)][PF₆] (μM)

Absorbance *vs* Concentration of Purified [(κ³-tpm)RuCl(dppm)][PF₆] for HeLa Cells (Trial 4)

IC₅₀ = > 50 μM

Concentration of [(κ³-tpm)RuCl(dppm)][PF₆] (μM)

MCF-7 Cancer Cells Exposed to [(κ^3-tpm)RuCl(dppe)][PF$_6$] (6)

Absorbance *vs* Concentration of [(κ^3-tpm)RuCl(dppe)][PF$_6$] for MCF-7 Cells (Trial 1)

IC$_{50}$ = 8.45µM

Absorbance *vs* Concentration of [(κ^3-tpm)RuCl(dppe)][PF$_6$] for MCF-7 Cells (Trial 2)

IC$_{50}$ = 7.8 µM

100

HeLa Cancer Cells Exposed to [(κ³-tpm)RuCl(dppe)][PF₆] (6)

Absorbance *vs* Concentration of [(κ³-tpm)RuCl(dppe)][PF₆] for HeLa Cells (Trial 1)

IC₅₀ = 4.0 μM

Absorbance *vs* Concentration of [(κ³-tpm)RuCl(dppe)][PF₆] for HeLa Cells (Trial 2)

IC₅₀ = 4.0μM

MCF-7 Cancer Cells Exposed to [(κ³-tpm)RuCl(dppp)][PF₆] (7)

Absorbance *vs* Concentration of [(κ³-tpm)RuCl(dppp)][PF₆] for MCF-7 Cells (Trial 1)

IC$_{50}$ = 2.8 µM

Concentration of [(κ³-tpm)RuCl(dppp)][PF₆] (µM)

Absorbance *vs* Concentration of [(κ³-tpm)RuCl(dppp)][PF₆] for MCF-7 Cells (Trial 2)

IC$_{50}$ = 2.9 µM

Concentration of [(κ³-tpm)RuCl(dppp)][PF₆] (µM)

Absorbance *vs* Concentration of [(κ³-tpm)RuCl(dppp)][PF₆]
for HeLa Cells (Trial 1)

IC₅₀ = 5.95 µM

Concentration of [(κ³-tpm)RuCl(dppp)][PF₆] (µM)

Absorbance *vs* Concentration of [(κ³-tpm)RuCl(dppp)][PF₆]
for HeLa Cells (Trial 2)

IC₅₀ = 7.8 µM

Concentration of [(κ³-tpm)RuCl(dppp)][PF₆] (µM)

103

MCF-7 Cancer Cells Exposed to [(κ^3-tpm)RuCl(dppb)][PF$_6$] (8)

**Absorbance *vs* Concentration of [(κ^3-tpm)RuCl(dppb)][PF$_6$]
for MCF-7 Cells (Trial 1)**

IC$_{50}$ = 2.9 µM

Concentration of [(κ^3-tpm)RuCl(dppb)][PF$_6$] (µM)

**Absorbance *vs* Concentration of [(κ^3-tpm)RuCl(dppb)][PF$_6$]
for MCF-7 Cells (Trial 2)**

IC$_{50}$ = 2.8 µM

Concentration of [(κ^3-tpm)RuCl(dppb)][PF$_6$] (µM)

HeLa Cancer Cells Exposed to [(κ³-tpm)RuCl(dppb)][PF₆] (8)

Absorbance *vs* Concentration of [(κ³-tpm)RuCl(dppb)][PF₆] for HeLa Cells (Trial 1)

IC₅₀ = 6.0 µM

Absorbance *vs* Concentration of [(κ³-tpm)RuCl(dppb)][PF₆] for HeLa Cells (Trial 2)

IC₅₀ = 5.6 µM

105
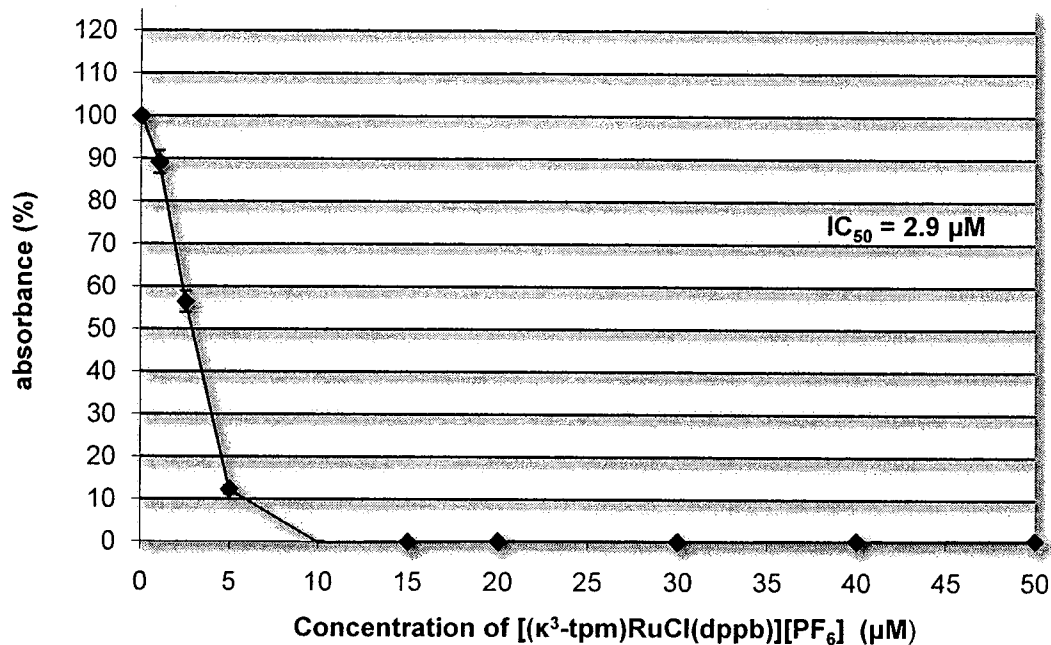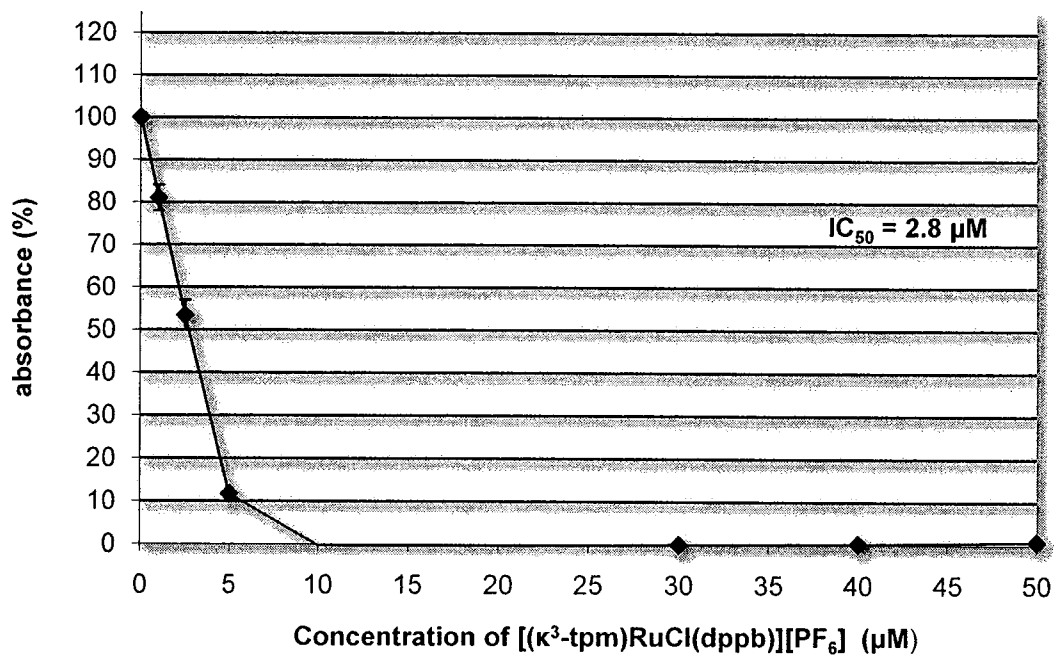
MCF-7 Cancer Cells Exposed to $[(\eta^6$-p-cymene)RuCl(dppp)]Cl

Absorbance vs Concentration of $[(\eta^6$-p-cymene)RuCl(dppp)]Cl for MCF-7 Cells (Trial 1)

$IC_{50} = 0.8 \ \mu M$

Concentration of $[(\eta^6$-p-cymene)RuCl(dppp)]Cl (μM)

Absorbance vs Concentration of $[(\eta^6$-p-cymene)RuCl(dppp)]Cl for MCF-7 Cells (Trial 2)

$IC_{50} = 0.8 \mu M$

Concentration of $[(\eta^6$-p-cymene)RuCl(dppp)]Cl (μM)

HeLa Cancer Cells Exposed to [(η⁶-p-cymene)RuCl(dppp)]Cl

Absorbance vs Concentration of [(η⁶-p-cymene)RuCl(dppp)]Cl for HeLa Cells (Trial 1)

IC_{50} = 1.3 µM

absorbance (%)

Concentration of [(η⁶-p-cymene)RuCl(dppp)]Cl (µM)

Absorbance vs Concentration of [(η⁶-p-cymene)RuCl(dppp)]Cl for HeLa Cells (Trial 2)

IC_{50} = 1.4 µM

absorbance (%)

Concentration of [(η⁶-p-cymene)RuCl(dppp)]Cl (µM)

MCF-7 Cancer Cells Exposed to Cisplatin

**Absorbance *vs* Concentration of Cisplatin
for MCF-7 Cells (Trial 1)**

$IC_{50} = > 20 \ \mu M$

**Absorbance *vs* Concentration of Cisplatin
for MCF-7 Cells (Trial 2)**

$IC_{50} = > 20 \ \mu M$

Absorbance *vs* Concentration of Cisplatin
for MCF-7 Cells (Trial 3)

IC_{50} = 18.4 µM

HeLa Cancer Cells Exposed to Cisplatin

Absorbance *vs* Concentration of Cisplatin
for HeLa Cells (Trial 1)

IC_{50} = 11.8 µM

Absorbance *vs* Concentration of Cisplatin for HeLa Cells (Trial 2)

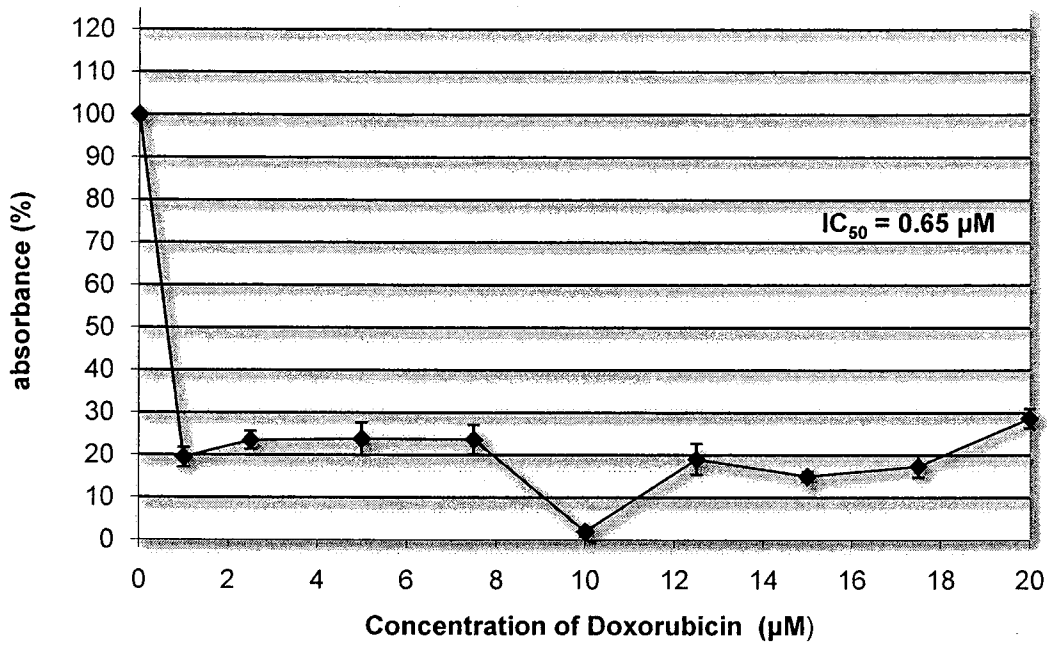$IC_{50} = 13.0$ μM

Concentration of Cisplatin (μM)

MCF-7 Cancer Cells Exposed to Doxorubicin

Absorbance *vs* Concentration of Doxorubicin for MCF-7 Cells (Trial 1)

$IC_{50} = 0.8$ μM
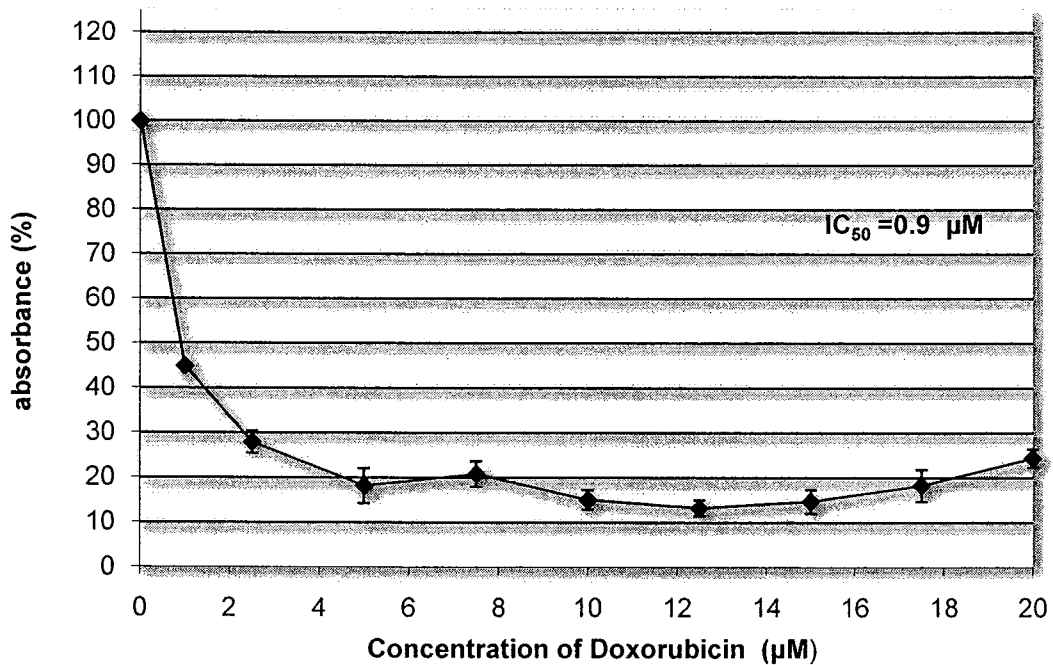
Concentration of Doxorubicin (μM)

**Absorbance *vs* Concentration of Doxorubicin
for MCF-7 Cells (Trial 2)**

$IC_{50} = 0.65$ µM

HeLa Cancer Cells Exposed to Doxorubicin

**Absorbance *vs* Concentration of Doxorubicin
for HeLa Cells (Trial 1)**

$IC_{50} = 0.9$ µM

111

Absorbance *vs* Concentration of Doxorubicin for HeLa Cells (Trial 2)

$IC_{50} = 1.15 \ \mu M$